The multi-component mantle source of Roman province ultrapotassic magmas revealed by melt inclusions

Bracco Gartner, Antoine J.J.; Nikogosian, Igor K.; Davies, Gareth R.; Koornneef, Janne M.

published in
Geochimica et Cosmochimica Acta
2023

DOI (link to publisher)
10.1016/j.gca.2023.06.012

document version
Publisher's PDF, also known as Version of record

Geochimica et Cosmochimica Acta 355 (2023) 266–281

Contents lists available at ScienceDirect

Geochimica et Cosmochimica Acta

journal homepage: www.elsevier.com/locate/gca

The multi-component mantle source of Roman province ultrapotassic magmas revealed by melt inclusions

Antoine J.J. Bracco Gartner [a,*], Igor K. Nikogosian [a,b], Gareth R. Davies [a], Janne M. Koornneef [a]

[a] Faculty of Science, Vrije Universiteit Amsterdam, De Boelelaan 1085, 1081 HV Amsterdam, the Netherlands
[b] Department of Earth Sciences, Utrecht University, Princetonlaan 8a, 3584 CB Utrecht, the Netherlands

ARTICLE INFO

Associate editor: Rosemary Hickey-Vargas

Keywords:
Ultrapotassic magmatism
Mantle source
Melt inclusions
Sr-Nd-Pb isotopes
Roman magmatic province

ABSTRACT

A key effect of subduction is the upward infiltration of slab-derived melts and fluids to create a chemically and lithologically heterogeneous region in the mantle wedge. Magmatism within the post-subduction setting of peninsular Italy is derived from a sediment-metasomatised lithospheric mantle source, with primitive products recording substantial temporal and spatial variations in the nature and extent of metasomatism. The Roman magmatic province, in central Italy, is host to ultrapotassic (HKS), leucite-bearing magmas that require source modification that is not yet well-constrained in terms of mineralogy and sediment provenance. Here, we present the chemistry and Sr-Nd-Pb isotope compositions of melt inclusions in forsterite-rich olivine (Fo_{88-92}) from three key Roman volcanic centres (Vulsini, Sabatini, Alban Hills) to characterise the metasomatic imprint of their mantle sources. The melt inclusion suites (Vulsini HKS, Vulsini melilite-bearing HKS, Sabatini HKS, Alban Hills HKS) have clear differences in major-element (K, Ca, Al, P, Ti), volatile (F, Cl, B, Be), trace-element (e.g., Rb, Sr/Y, Th/Nb), and radiogenic-isotope ($^{87}Sr/^{86}Sr$) compositions that reflect the diversity of the primary melts beneath the region. For each suite, the extraction of melt batches from different domains in a heterogeneous (veined) source rock with different compositions and mineralogies can explain the chemical characteristics of the melts. At least three metasomatic vein types are required to form the respective parental melts and we infer phase assemblages consisting of phlogopite + Ca-amphibole + clinopyroxene ± apatite. The Sr-isotope differences between Vulsini melilite-bearing HKS and Vulsini and Sabatini HKS require at least two distinct metasomatic events to have occurred beneath the Roman province. These events need not be associated with two distinct subduction systems. Instead, we infer that different metasomatic agents could have originated under different P-T-t conditions from different domains in the same subducting slab.

1. Introduction

The liberation of melts and fluids from the down-going slab during subduction is one of the chief causes of chemical and lithological heterogeneity in the mantle. This heterogeneity, often envisioned in the form of a veined mantle (Hanson, 1977; Allègre and Turcotte, 1986; Foley, 1992), may be tapped during melt generation in a post-collisional setting, as these metasomatically-induced portions characteristically have lower melting temperatures than the surrounding wall-rock due to the presence of more fusible and/or hydrous phases. The exact nature of a metasomatised mantle source region, in terms of geochemistry and mineralogy, varies according to (1) the nature of the subducted material (Plank and Langmuir, 1998; Plank, 2014), (2) the P-T conditions at the slab-wedge interface during melt/fluid liberation (Class et al., 2000; Manning, 2004), (3) flow differentiation during upward infiltration of metasomatic agents (Harte, 1987; Spandler and Pirard, 2013), and (4) the melting and mixing processes occurring during melt extraction (Stracke and Bourdon, 2009; Rudge et al., 2013). Since all factors may vary, and direct samples of such source regions are scarce, it has proven difficult to pinpoint the characteristics of these portions of the mantle, especially in post-collisional settings.

The recent post-subduction volcanism of peninsular Italy, in the central-western Mediterranean region, involves one of the most complex mantle sources worldwide. Italy's present-day tectonic configuration is the result of plate convergence involving continental Europe, the extending western Mediterranean realm, and subducting Adriatic and Ionian lithosphere (Wortel and Spakman, 2000; Carminati et al., 2012; van Hinsbergen et al., 2014, 2020). The Quaternary post-collisional

* Corresponding author.
E-mail address: a.j.j.braccogartner@vu.nl (A.J.J. Bracco Gartner).

https://doi.org/10.1016/j.gca.2023.06.012
Received 31 October 2022; Accepted 12 June 2023
Available online 15 June 2023

magmatic products of the Italian mainland are potassium-rich and show trace-element and radiogenic isotope signatures that collectively point to the partial melting of upper mantle domains affected by subduction-related metasomatism (Conticelli and Peccerillo, 1992; Boari et al., 2009b; Conticelli et al., 2015). The magmas parental to the erupted products exhibit extreme compositional variability in space and time, at least partially reflecting variations in the subducted material in their mantle sources (Peccerillo, 1999; Conticelli et al., 2002; Avanzinelli et al., 2009; Conticelli et al., 2015).

Although extensive studies of Italian mafic volcanic rocks have used radiogenic isotopes and trace-element data to argue for recycled slab-derived material in the melt source, bulk magmas may be subjected to variable degrees of assimilation and homogenisation at crustal levels, which conceal the true composition and heterogeneity of the mantle source. The extreme geochemical and isotopic compositions of the Roman magmas cannot be controlled by these secondary processes alone (e.g., Conticelli et al., 2010, 2015), but to obtain samples of (near-)primary magma compositions we target melt inclusions (MIs) in forsteritic olivine. Olivine-hosted MIs are small parcels of magma that, after entrapment during the earliest stages of magma evolution, are shielded from subsequent magma mixing, assimilation and contamination on the way to the Earth's surface (e.g., Sobolev, 1996; Danyushevsky et al., 2002a). Hence, MIs allow the degree and origin of compositional heterogeneity of Italian mantle sources to be interrogated with increased resolution (Metrich et al., 1998; Nikogosian and van Bergen, 2010; Rose-Koga et al., 2012; Koornneef et al., 2019).

Here we present major-, volatile-, and trace-element data and coupled Sr-Nd-Pb isotope data on individual olivine-hosted melt inclusions from the ultrapotassic series (HKS) magmas of the Roman magmatic province in central Italy. The aims of this study are to (1) characterise and explain the compositional diversity of melts parental to Roman-type magmas; (2) constrain the metasomatic imprint of the mantle source and its control on melt compositions; (3) probe the nature and origin of the metasomatic agents; (4) place the metasomatic history and magma genesis in the regional geodynamic context (Fig. 1); and, ultimately, to (5) further the understanding of the origin of ultrapotassic volcanism in post-collisional settings.

2. Geodynamic and magmatic setting

The current post-collisional configuration of Italy is the product of a complex tectonic history involving (1) the south- to eastward subduction of Tethyan oceanic lithosphere in the north (the "Alpine" subduction) during the Cretaceous to Oligocene, and (2) since the late Eocene the southwest to westward subduction of the oceanic and continental Adriatic and oceanic Ionian lithosphere below the central and southern regions (the "Apennine" subduction) accompanied by eastward rollback (Fig. 1; Wortel and Spakman, 2000; Spakman and Wortel, 2004; Carminati et al., 2012; Giacomuzzi et al., 2012). Subduction is ongoing only in the Calabrian Arc, with active volcanic activity in the Campanian area and on Sicily and the Aeolian Islands. Seismic tomography has been used to identify fossil and actively subducting slabs beneath Italy, and testifies to the rollback, tearing, and detachment of slabs and lithospheric delamination that accompanied subduction of the Adriatic lithosphere in the Apennine subduction zone (Fig. 1b; Serri et al., 1993; Wortel and Spakman, 2000; Faccenna et al., 2001; Giacomuzzi et al., 2012; Chiarabba and Chiodini, 2013). The slab windows, tears and detachments provide a pathway for relatively hot asthenosphere to rise and transfer the heat required to induce melting of mantle domains above the slab, which have been affected by subduction processes and addition of material from the slab (Spakman and Wortel, 2004; Rosenbaum et al., 2008).

The resulting volcanism on the Italian mainland during the Quaternary has formed (ultra)potassic volcanic complexes that are aligned along the border of the Tyrrhenian Sea, stretching from Tuscany down to Campania (Fig. 1a). The predominantly potassium-rich and

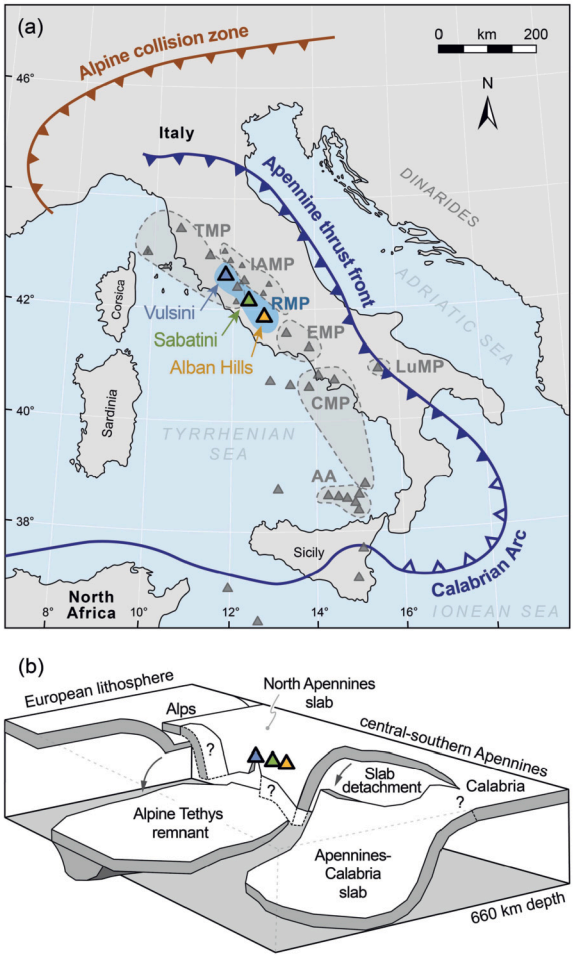

Fig. 1. Geodynamic and magmatic setting of Italy. (a) Map of Italy with the locations of Quaternary volcanic centres (triangles) and magmatic provinces (shaded areas) (redrawn after Conticelli et al., 2007; Nikogosian et al., 2016; Peccerillo, 2017). TMP = Tuscan magmatic province; IAMP = Intra-Apennine magmatic province; RMP = Roman magmatic province; EMP = Ernici-Roccamonfina magmatic province; LuCMP = Lucanian magmatic province; CMP = Campanian magmatic province (including Stromboli); AA = Aeolian Arc. Lines with sawteeth denote the Alpine, Apennine, and Calabrian subduction systems. (b) Schematic illustration of the slabs in the upper mantle beneath Italy based on seismic tomography (modified after Spakman and Wortel, 2004), showing the approximate locations of the studied Roman volcanic centres.

"subduction-type" signature of the magmas is associated with extraction from mantle domains metasomatised by melts and/or fluids derived from subducted sediments and/or lithosphere (Boari et al., 2009b; Avanzinelli et al., 2009; Carminati et al., 2012; Conticelli et al., 2015; Peccerillo, 2017). The regional N-S trend in trace-element and radiogenic isotope signatures of the mafic Italian volcanics is interpreted to reflect a change in the amount and/or nature of the metasomatic agents (Conticelli and Peccerillo, 1992; Serri et al., 1993; Peccerillo, 1999; Conticelli et al., 2002; Peccerillo, 2017), possibly accompanied by a southward increase in the involvement of an asthenospheric mantle component (Beccaluva et al., 1991; Gasperini et al., 2002). At the scale of individual volcanic districts and complexes, the large spectrum of often coexisting magma compositions—calc-alkaline, shoshonitic, potassic, ultrapotassic and lamproitic, among others—can be attributed to factors including (1) a heterogeneous pre-metasomatic mantle; (2) mantle heterogeneities resulting from (superimposed) metasomatic events; (3) progressive melt-extraction processes; and (4) crustal interaction (Foley, 1992; Peccerillo, 1999; Conticelli et al., 2004; Nikogosian et al., 2016; Peccerillo, 2017; Koornneef et al., 2019).

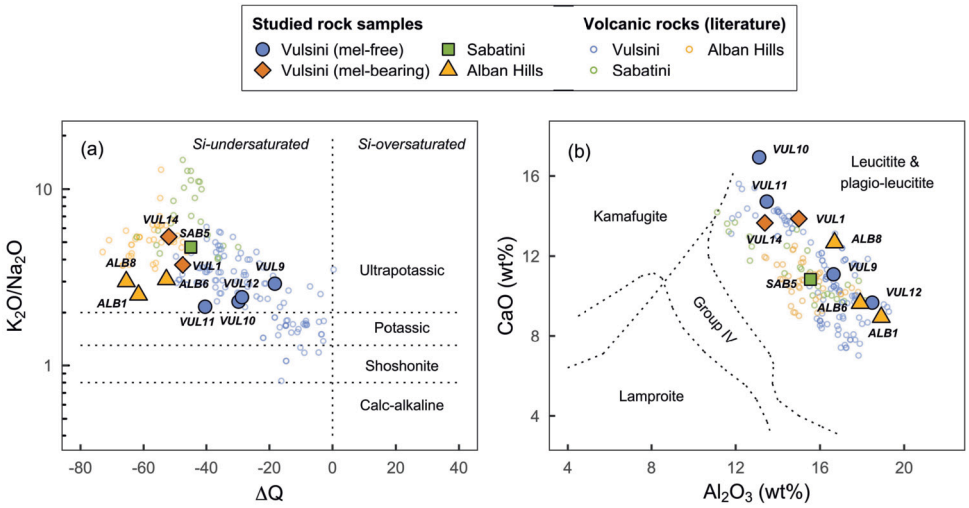

Fig. 2. Major-element contents of the Roman HKS rock samples. (a) ΔQ versus K_2O/Na_2O (Peccerillo, 2003). ΔQ is the algebraic sum of normative quartz minus normative undersaturated minerals (nepheline, leucite, kalsilite, olivine). (b) Al_2O_3 versus CaO (in wt%; Foley et al., 1987). Mafic rocks (MgO > 5 wt%) with LOI values < 3 wt% from the literature are plotted for comparison. Literature data: Vulsini (Brai et al., 1979; Civetta et al., 1984; Rogers et al., 1985; Conticelli et al., 1986, 1987, 1991; Conticelli and Peccerillo, 1992; Varekamp and Kalamarides, 1989; Vernia et al., 1995; Di Battistini et al., 1998, 2001; Gasperini et al., 2002; Avanzinelli et al., 2008); Sabatini (Conticelli et al., 1997; Gasperini et al., 2002; Sottili et al., 2012; Masotta et al., 2016); Alban Hills (Freda et al., 1997; Giordano et al., 2006; Conticelli et al., 2007; Avanzinelli et al., 2008; Boari et al., 2009a; Gaeta et al., 2009; Peccerillo et al., 2010; Di Rocco et al., 2012).

The Roman magmatic province in central Italy encompasses the volcanic centres of Vulsini, Vico, Sabatini, and Alban Hills (also known as Colli Albani) that were active between 800 and <20 ka (Peccerillo, 2017, and references therein). It is host to predominantly silica-undersatured, ultrapotassic (HKS) rocks, though lesser, nearly silica-saturated, shoshonitic (SHO) rocks also occur at Vulsini (Latera) and Vico (Peccerillo, 2017). The Roman magmatic province is situated between the Tuscan province to the north, where mantle-derived magmas are of lamproite–shoshonite–calc-alkaline association (Conticelli et al., 2010), and Ernici-Roccamonfina to the south, which represents a geographic and geochemical transition with products that share isotopic and geochemical affinity with the Roman province in the north and the Campanian and Aeolian provinces in the south (Nikogosian and van Bergen, 2010; Peccerillo, 2017).

3. Samples

The selected rock samples from the volcanic districts of Vulsini (n = 6), Sabatini (n = 1) and Alban Hills (n = 3) represent the least-evolved magmas of the Roman ultrapotassic series that carry olivine as a liquidus phase. The samples cover the compositional variability present in the most primitive ultrapotassic rocks of the Roman magmatic province. Their compositions, mineralogy, and further details are listed in Supplementary Table S1. All studied rocks classify as ultrapotassic (Peccerillo, 2003) and leucititic (Conticelli et al., 2015) (Fig. 2). The geochemical, mineralogical, and petrographical characteristics of the lava flows from which the samples are taken have previously been described in detail (Vulsini: e.g., Nappi et al. (1998); Di Battistini et al. (1998, 2001); Sabatini: e.g., Conticelli et al. (1997); Sottili et al. (2012, 2019); Alban Hills: e.g., Peccerillo et al. (1984); Giordano et al. (2006); Boari et al. (2009a)).

Samples from Vulsini are from the complexes of Bolsena and Montefiascone. Bolsena samples are from Trebianello (VUL-1) and Castel Cellesi (VUL-9) (Nappi et al., 1998). Montefiascone samples are from Forcinella (VUL-10), Orto Piatto (VUL-11), the Mentuccia area (VUL-12), and Fosso Feltricci (VUL-14) (Di Battistini et al., 2001). Compared to VUL-9 and VUL-12, samples VUL-10 and VUL-11 have higher CaO and lower Al_2O_3 (Fig. 2b), but all four belong to the HKS. We distinguish VUL-1 and VUL-14 from the former group based on the occurrence of melilite and associated elemental enrichments and more pronounced silica-undersaturation. These compositions will be referred to as melilite-bearing HKS ("mel-HKS" in short).

Sabatini sample SAB-5 is from the Monte Maggiore scoria cone (206 ± 7 ka; Sottili et al., 2010) of the Sacrofano volcano. Like all mafic rocks from Sabatini (Fig. 2), it belongs to the HKS.

The three samples from Alban Hills (ALB-1,6,8) are from the Alban Hills HKS. ALB-1 and ALB-6 are from Villa Senni lava flows near Campoleone and at Quarto Roncigliano, respectively (Peccerillo et al., 1984). Both samples belong to the Villa Senna eruptive unit, dated at 365 ± 4 ka (Marra et al., 2009). ALB-8 is from the Vallerano lava flow (Peccerillo et al., 1984) (457 ± 5 ka; age after Karner et al., 2001).

4. Methods

Whole-rocks were crushed and powdered to determine their compositions by X-ray fluorescence spectrometry (major elements) and inductively coupled plasma mass spectrometry (ICP-MS; trace elements) using a Philips PW1404/10 and Thermo Electron X-series II ICP-MS, respectively, at the Vrije Universiteit Amsterdam.

Olivine fractions were isolated after sieving using gravimetric heavy-liquid separation and olivine phenocrysts were handpicked using a binocular microscope. Forsterite-rich olivine grains containing MIs were selected to determine the crystallisation conditions through experimental and analytical work. The MIs were rehomogenised and quenched using a high-temperature heating/quenching stage at the Vrije Universiteit Amsterdam following procedures outlined in Nikogosian et al. (2002). Olivines were mounted in epoxy and polished on one side, typically until the melt inclusions were exposed at the surface, for major-, trace-, and volatile-element analysis by electron microprobe analysis (EPMA), laser ablation (LA-)ICP-MS and/or secondary ion mass spectrometry (SIMS).

Major-element data on olivines, spinel inclusions, and rehomogenised MIs, as well as volatile elements (Cl, S, F) in MIs, were obtained using a JEOL JXA-8600 SuperProbe at Utrecht University, operated in wavelength dispersive (WDS) mode, following the procedure described in de Hoog et al. (2001). Natural minerals, metals, and synthetic oxides were used as calibration standards.

The major-element compositions of the MIs were corrected for post-entrapment "Fe-loss" (Danyushevsky et al., 2000, 2002a) using the conventional method of Danyushevsky et al. (2000), assuming uniform

initial FeO contents corresponding to that of the respective host rocks. The olivine-melt equilibrium model of Ford et al. (1983) was used, using Fe^{2+}/Fe^{3+} ratios in the melt as estimated from coexisting Cr-spinel inclusions in olivine, using the spinel-melt equilibria of Maurel and Maurel (1982). These corrections chiefly affect MgO and FeO concentrations; the effects on other major-element oxides are insignificant so that overall geochemical trends and compositional variability remain unaffected. The temperature of olivine-MI equilibrium, i.e., the entrapment temperature, was calculated using the model of Danyushevsky et al. (2000). All these calculations were performed using `Petrolog3` (Danyushevsky and Plechov, 2011).

Trace-element concentrations, including B, Be, and F, in rehomogenised MIs were obtained by SIMS using a CAMECA IMS4f at the Institute of Microelectronics in Yaroslavl, Russia, following techniques and procedures reported by Danyushevsky and Sobolev (1996) and Portnyagin et al. (2007) and operational details listed in Nikogosian et al. (2016). A calibration curve for glass standards ATHO-Ga (Jochum et al., 2006) and NIST SRM 610 (Jochum et al., 2011) was used to calculate element concentrations based on the ratio of the respective isotopes to ^{30}Si.

The trace-element contents of additional (re- and unhomogenised) melt inclusions were determined by LA-ICP-MS using a 193-nm GeoLas 200Q Excimer laser ablation system, coupled to a Micromass Platform quadrupole ICP-MS instrument at Utrecht University, following procedures described in Mason et al. (2008) and the operational details listed in Nikogosian et al. (2016). Quantitative concentrations were calculated using NIST SRM 610 as a calibration standard (Jochum et al., 2011), using Ca in the MI as measured by EPMA (for rehomogenised MIs) or Ca in the host-rock (for unhomogenised MIs) as an internal standard. USGS reference glass BCR-2G was used as a secondary standard throughout analysis.

Coupled Sr-Nd-Pb isotope compositions were obtained by thermal ionisation mass spectrometry (TIMS) at the Vrije Universiteit Amsterdam. Selected MI-bearing olivines were freed of adhering groundmass and/or possible surface contaminants by leaching in 2 N HF (30–60 min) and 2 N HNO_3 (30–60 min) in an unheated ultrasonic bath prior to digestion. The clean olivines were dissolved in Teflon vials in a mixture of concentrated HF and HNO_3. The Pb fraction was separated using 50 µl Bio-Rad AG1-X8 200–400 mesh resin following the methods of Klaver et al. (2016) using a single column pass, after which the Sr and Nd fractions were isolated using the miniaturised technique of Koornneef et al. (2015). Total procedural blanks processed during this study gave averages of 17.7 pg for Sr ($n = 4$), 0.13 pg for Nd ($n = 4$), and 2.1 pg for Pb ($n = 2$). TIMS analyses were performed using a Thermo Scientific Triton *Plus* equipped with four 10^{13} Ω amplifiers using the techniques for Sr-Nd as described in Koornneef et al. (2014, 2015), and the double-spike Pb technique as outlined in Klaver et al. (2016). Nd and Pb were typically run to exhaustion. Similarly-sized aliquots of rock reference materials USGS AGV-1 and GSJ JB-2 were used as secondary standards and were processed alongside the unknowns, yielding Sr-Nd-Pb data in agreement with the GeoReM preferred values (Jochum et al., 2006) (Supplementary Table S5).

5. Results

5.1. Mineralogy

5.1.1. Olivine phenocrysts

The forsterite contents of olivine phenocrysts (Fo = Mg/(Mg+Fe) in mol%) (Supplementary Table S2) range from Fo_{85} to Fo_{92} in Vulsini mel-HKS, Fo_{76} to Fo_{92} in Vulsini HKS, Fo_{86} to Fo_{91} in Sabatini HKS, and Fo_{85} to Fo_{90} in Alban Hills HKS. Less Fo-rich olivines occur in all studied localities, but were not selected for analysis.

The largest compositional difference between the Vulsini mel-HKS and HKS olivines is in CaO contents (Fig. 3a). Vulsini mel-HKS olivines have on average higher CaO values (0.4–0.8 wt%; mean = 0.6 wt%) than Vulsini HKS olivines (0.2–0.5 wt%; mean = 0.35 wt%), with the two groups overlapping between 0.4–0.5 wt%. Although their MnO fractionation trends start at similar values, the trend of mel-HKS olivines just below Fo_{90} is noticeably steeper than that of HKS olivines (Fig. 3b). Their NiO contents (Fig. 3c) around Fo_{90-92} are similar, ranging chiefly between 0.15 and 0.35 wt%.

Sabatini HKS olivines have relatively restricted CaO contents, between 0.4 and 0.5 wt%, overlapping the higher and lower parts of the Vulsini HKS and mel-HKS suites, respectively (Fig. 3a). They have NiO and MnO contents similar to the other series (Fig. 3).

Alban Hills HKS olivines contain two sub-populations in terms of CaO contents, with samples ALB-1,8 having CaO values of 0.45–0.55 wt%, and sample ALB-6 having relatively low CaO contents, of ~ 0.3 wt%. Most of the Alban Hills HKS olivines group together at slightly higher SiO_2 (~ 41.5 wt%) than the Vulsini and Sabatini olivines (39–41 wt%) around Fo_{90}. The Alban Hills olivines exhibit no differences in NiO and MnO contents (Fig. 3), and are comparable to those of Vulsini and Sabatini.

5.1.2. Spinel inclusions in olivine

Cr-spinel inclusions were identified in forsteritic olivines from all samples (Supplementary Table S3). Their Mg# (Mg/(Mg+Fe^{2+}) in mol%) range from 58–66 mol% for Vulsini mel-HKS, 53–70 mol% for Vulsini HKS, 40–72 mol% for Sabatini, and 48–68 mol% for Alban Hills. In general, the Fo contents of the host olivines correlate positively with Mg#. Other expected covariations, such as with Fe^{2+}/Fe^{3+}, Fe^{3+}, and TiO_2, are not apparent because of the limited interval of olivine Fo contents (mainly 90–92 mol%).

Vulsini mel-HKS Cr-spinels are distinct from those of Vulsini HKS in having higher Cr# (Cr/(Cr+Al); 73–82 vs. 55–75 mol%; Fig. 3d), Fe^{3+} (0.23–0.30 vs. 0.10–0.28 cation frac), and lower Al_2O_3 (8–11 vs. 12–21 wt%), V_2O_3 (0.09–0.14 vs. 0.12–0.22 wt%), and Fe^{2+}/Fe^{3+} (1.2–1.6 vs. 1.3–3.5).

The Cr-spinels of Sabatini HKS exhibit values for Cr# (75–80 mol%; Fig. 3d), Al_2O_3 (8–11 wt%), and TiO_2 (0.4–0.6 wt%) that are generally similar to Vulsini mel-HKS spinels. Fe^{2+}/Fe^{3+} (1.5–2.1) and V_2O_3 (0.12–0.17 wt%) are somewhat higher than that of Vulsini mel-HKS, the opposite of which is true for Fe^{3+} (0.17–0.23 cation frac).

Alban Hills HKS Cr-spinels have two sub-populations in terms of Cr# (73–77 vs. 57–65 mol%; Fig. 3d) and Al_2O_3 (11–12 vs. 16–22 wt%), of which the former shows less scatter. Collectively, their TiO_2 fall on the higher end of the spectrum (0.55–0.90 wt%), and together with Fe^{3+} (0.15–0.25 cation frac) and Fe^{2+}/Fe^{3+} (1.5–2.7), Cr#, Cr_2O_3, and Al_2O_3, these spinels generally plot between the spinels from the other localities.

5.2. Melt inclusions in olivine

Magmatic inclusions were identified in forsteritic olivines from all localities (Supplementary Table S4), though Fo-rich olivines and therefore MIs are rare at Alban Hills. The homogenisation temperatures recorded during the high-temperature microthermometric heating/quenching experiments give an estimate of the temperatures at which the MIs were trapped during host-olivine crystallisation (Nikogosian et al., 2002), and are 1220–1300 °C for Vulsini HKS (Fo_{90-92}), 1180–1240 °C for Vulsini mel-HKS (Fo_{88-91}), 1220–1250 °C for Sabatini HKS (Fo_{90}), and 1250 °C for Alban Hills (Fo_{90}, $n = 3$). These values are in agreement with the calculated olivine-MI equilibrium temperatures (1240–1330 °C for Vulsini HKS (Fo_{90-92}), 1160–1280 °C for Vulsini mel-HKS (Fo_{89-91}), 1240–1280 °C for Sabatini HKS (Fo_{90-91}), and 1270 °C for Alban Hills (Fo_{90})), the main difference being that the maximum calculated values for each suite are about 10–20 °C higher.

5.2.1. Major elements

The MI suites show considerable major-element differences, particularly between Vulsini mel-HKS, Sabatini HKS, and Vulsini HKS (Fig. 4).

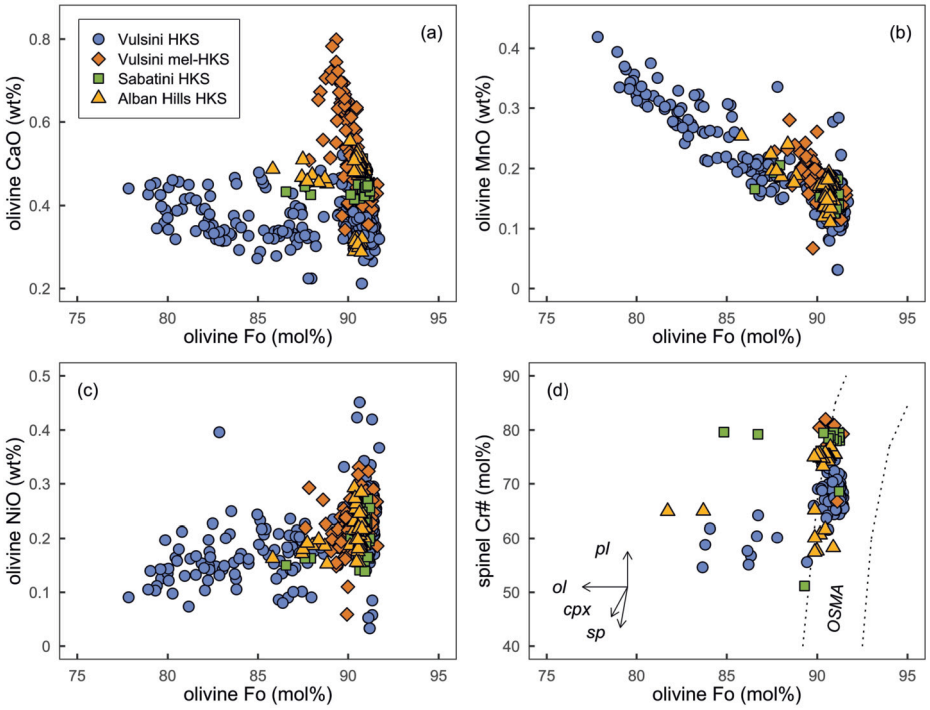

Fig. 3. Major-element contents of Roman HKS olivines and Cr-spinels. Olivine forsterite contents (Fo in mol%) versus (a) CaO, (b) MnO, and (c) NiO (in wt%) in olivine, and (d) Cr# (Cr/(Cr+Al) in mol%) in coexisting Cr-spinel inclusions. Olivine-spinel mantle array (OSMA) in (d) after Arai (1994). Black arrows in (d) indicate expected fractionation trends for olivine (ol), clinopyroxene (cpx), spinel (sp), and plagioclase (pl) from Smith and Leeman (2005).

Compared to Vulsini HKS, the mel-HKS inclusions have higher K_2O, P_2O_5, TiO_2, CaO (albeit very scattered), and lower SiO_2 and MgO. Sabatini HKS inclusions are also distinct from Vulsini HKS with higher K_2O, P_2O_5, and TiO_2, and lower SiO_2 and MgO, and are in these respects similar to Vulsini mel-HKS. The limited number of MIs from Alban Hills are more similar to Vulsini HKS, but with relatively low K_2O, and somewhat higher SiO_2 and MgO.

In the most primitive inclusions, i.e., those hosted by olivines with Fo contents above 88 mol%, the variability in K_2O appears to be associated with variations in several other major-element oxides. Higher K_2O tends to be associated with higher CaO, Al_2O_3 (except Sabatini HKS), P_2O_5, TiO_2 (Fig. 4), and lower SiO_2 and MgO (not shown). Most striking is the large compositional variability within the Vulsini mel-HKS group, particularly in terms of CaO (8–17 wt%), Al_2O_3 (13–18 wt%), P_2O_5 (0.5–1.4 wt%), and TiO_2 (0.8–1.4 wt%).

5.2.2. Volatile elements

Most of the volatiles also vary with K_2O (Fig. 5). Particularly the MIs from Vulsini mel-HKS and Sabatini HKS, with the highest K_2O contents, have very enriched and variable volatile concentrations. Vulsini mel-HKS have high B (70–200 μg/g), Be (8–11 μg/g), F (2700–6500 μg/g), Cl (400–800 μg/g), and SO_3 concentrations (1500–6600 μg/g) compared to Vulsini HKS. Sabatini HKS show ranges for B, F, and SO_3 that are similar to Vulsini mel-HKS, though Be (8–14 μg/g) and F contents (1600–8500 μg/g) are on average noticeably higher in Sabatini. Alban Hills HKS, albeit small in sample size (n = 2–4), are generally similar to Vulsini HKS.

5.2.3. Trace elements

The trace-element compositions of the MIs from the different host-rock series are also distinct (Fig. 6). The primitive mantle-normalised trace-element patterns demonstrate the enrichment of Vulsini mel-HKS compared to HKS, and the variability of MI compositions compared to the host rocks. In the most forsteritic olivines (Fo > 88 mol%), strong positive covariations exist between K_2O and absolute trace-element abundances, such as the rare-earth elements (REEs), Sr, Cs, Zr, and Rb (Fig. 7a). Because the dataset contains more trace-element data than coupled major-trace element data, Rb is used as a proxy for K_2O to obtain a better view of melt diversity and compositional trends. Striking trace-element features are the higher Sr/Y, Th/Nb, and Th/Y values for Sabatini HKS compared to Vulsini HKS and Alban Hills HKS (Fig. 7b-d), whilst being comparable to Vulsini mel-HKS in Th/Nb and Th/Y. Vulsini mel-HKS are also marked by relatively enriched compositions, with higher Th/Nb and Th/Y values than Vulsini HKS. Sr/Y and Th/Y are similar for Vulsini mel-HKS and HKS. Alban Hills HKS is, perhaps partly due to the limited number of data points (n = 2), similar to Vulsini HKS for most trace-element ratios.

5.2.4. Sr-Nd-Pb isotopes

The radiogenic-isotope contents of the MIs hosted by olivines with Fo > 88 mol% are shown in Fig. 8. Though the variations are small for ultrapotassic rocks as a whole, there is a significant difference in $^{87}Sr/^{86}Sr$ values between Vulsini HKS and mel-HKS (0.7097–0.7103 vs. 0.7106–0.7107)—in the order of ~ 0.1%. In addition to the marked difference *between* the MI suites, they do not show $^{87}Sr/^{86}Sr$ covariations within the individual series (Fig. 8b-c). For Sabatini HKS, unlike their major- and trace-element features, the $^{87}Sr/^{86}Sr$ values overlap the range of Vulsini HKS rather than mel-HKS, although they have far less variation (0.7100–0.7102) than Vulsini HKS. Overall, the $^{87}Sr/^{86}Sr$ values of Vulsini mel-HKS are associated with high K_2O (Fig. 8a), and higher B, Be, and F, compared to Vulsini HKS (Fig. 8c-e), though Sabatini HKS show higher B, Be, and F concentrations at lower $^{87}Sr/^{86}Sr$ values than Vulsini mel-HKS.

The $^{143}Nd/^{144}Nd$ of the analysed MIs have no systematic relations with $^{87}Sr/^{86}Sr$ (Fig. 8f) or other elements that is outside of the analytical uncertainty. It appears as though Vulsini mel-HKS MIs fall on the lower end of the spectrum, and have on average lower $^{143}Nd/^{144}Nd$ than Vulsini HKS. Furthermore, there is one Sabatini HKS MI that has higher $^{143}Nd/^{144}Nd$ than the mafic whole-rock range (Fig. 8f). Fig. 8f also shows that the one Alban Hills MI for which Sr-Nd isotope data was obtained falls within the range of the whole rocks.

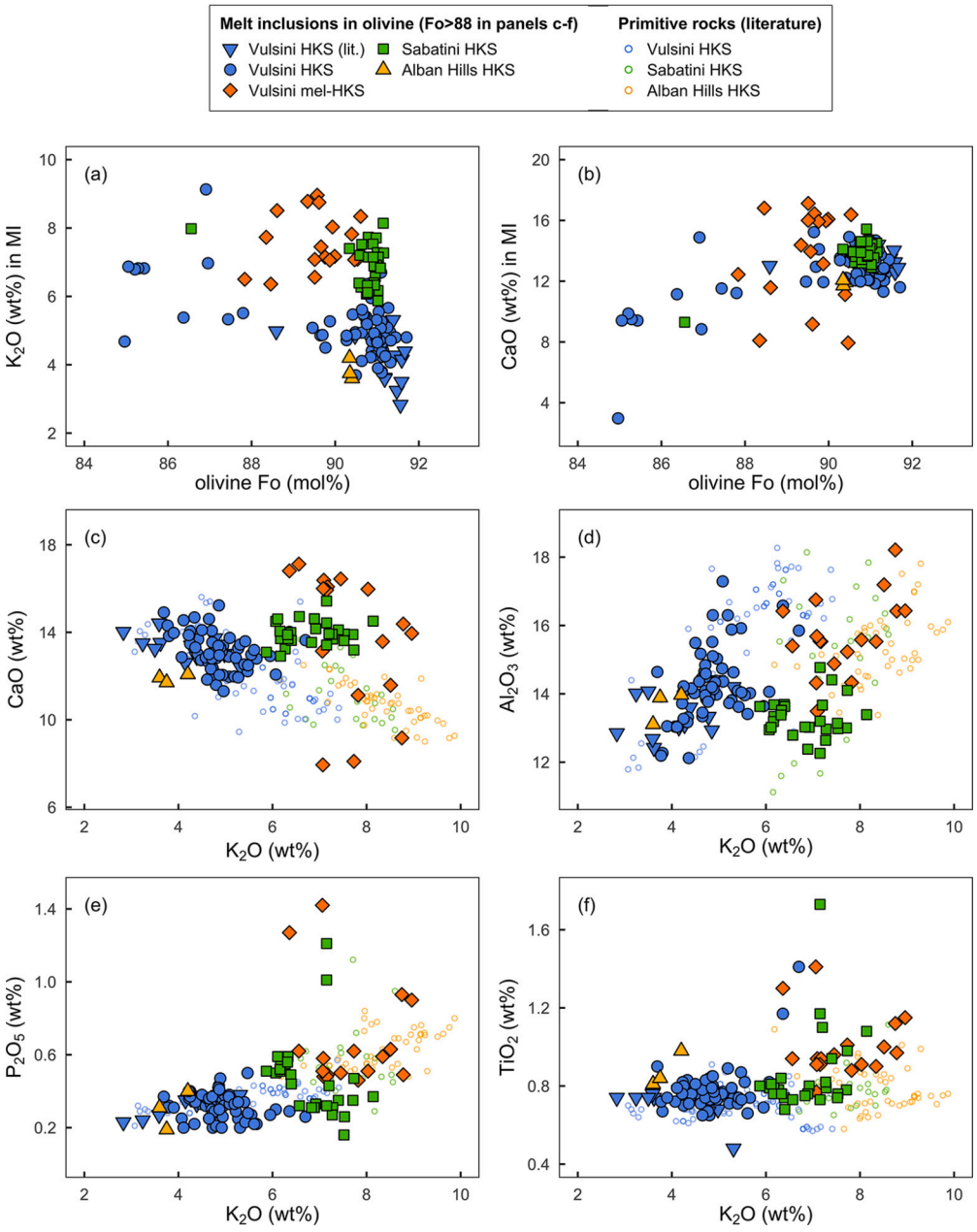

Fig. 4. Major-element contents of Roman HKS melt inclusions. Olivine forsterite contents (Fo in mol%) versus (a) K_2O and (b) CaO (in wt%) in the olivine-hosted melt inclusions (MIs). K_2O contents versus (c) CaO, (d) Al_2O_3, (e) P_2O_5, and (f) TiO_2 (in wt%) in melt inclusions hosted by olivines with Fo > 88 mol%. The Vulsini HKS MI data of Kamenetsky et al. (1995) and Metrich et al. (1998) (labelled "lit."), and Roman HKS primitive whole-rock data (MgO > 5 wt%, K_2O/Na_2O > 2, and LOI < 3 wt%; references as in Fig. 2) are shown for comparison.

The $^{206}Pb/^{204}Pb$ and $^{207}Pb/^{204}Pb$ values largely overlap the range of whole-rocks, though they are marked by slightly lower $^{208}Pb/^{204}Pb$ (Fig. 8g-h).

6. Discussion

6.1. Primitive melt batches recorded in forsterite-rich olivine

The major-, volatile-, trace-element and Sr-isotope compositions of the MIs trapped in olivines with high forsterite contents (Fo > 88 mol%) have no correlations with forsterite contents (Fig. 4ab). Because Fo decreases as the melt evolves and fractionally crystallises, the compositional diversity of the MIs at Fo > 88 mol% cannot be the result of such processes. Since olivine is the first principal liquidus phase to crystallise from typical Italian mantle-derived melts (alongside minor Cr-spinel; e.g., Nikogosian and van Bergen, 2010), the MIs trapped in these early-liquidus minerals are samples of melt batches from the deepest levels in the magmatic plumbing system. The fact that the MIs have such diverse compositions (Figs. 4–8) indicates that these primitive melt batches were chemically heterogeneous and distinct from one another. In addition, the preservation of this variability indicates that their host olivines must have crystallised relatively close to the melt source region, as any significant extraction of melt batches in channels would have inevitably accumulated them, averaging out any remaining heterogeneities. Therefore, we infer that the compositional variability of the MIs reflects the chemical heterogeneity of near-primary melts that were in equilibrium with the source rock. This variability—particularly in K_2O and associated covariations—provides new constraints on the source of the ultrapotassic melts of the Roman province.

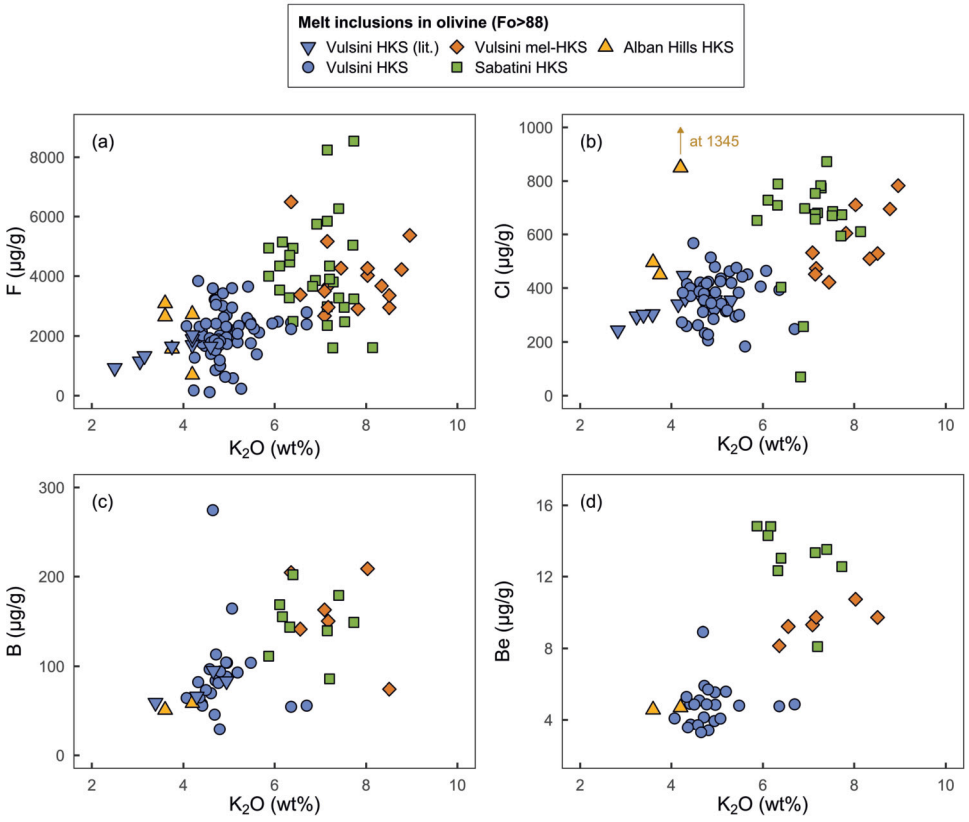

Fig. 5. Volatile-element contents of Roman HKS melt inclusions. K_2O contents versus (a) F, (b) Cl, (c) B, and (d) Be (in µg/g) in melt inclusions hosted by olivines with Fo > 88 mol%. The Vulsini HKS MI data of Kamenetsky et al. (1995) and Metrich et al. (1998) (labelled "lit.") are also shown.

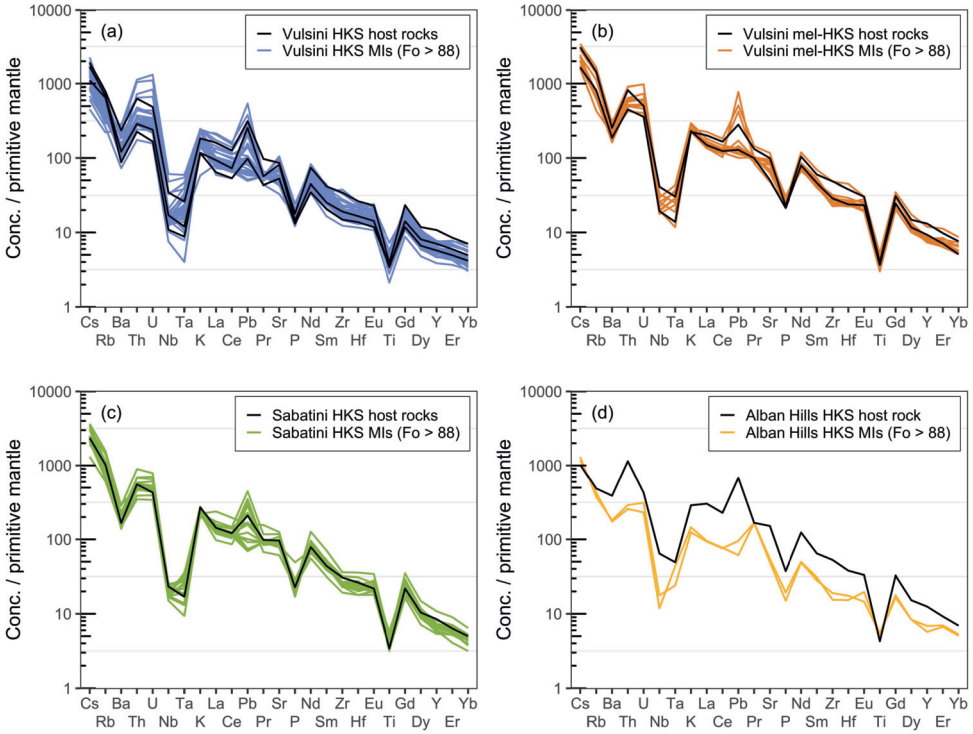

Fig. 6. Spider diagrams for Roman HKS melt inclusions. Primitive mantle-normalised (McDonough and Sun, 1995) trace-element patterns of MIs in olivines with Fo > 88 mol% from (a) Vulsini HKS, (b) Vulsini mel-HKS, (c) Sabatini HKS, and (d) Alban Hills HKS. Patterns of the host-rock samples (black lines) are shown for comparison.

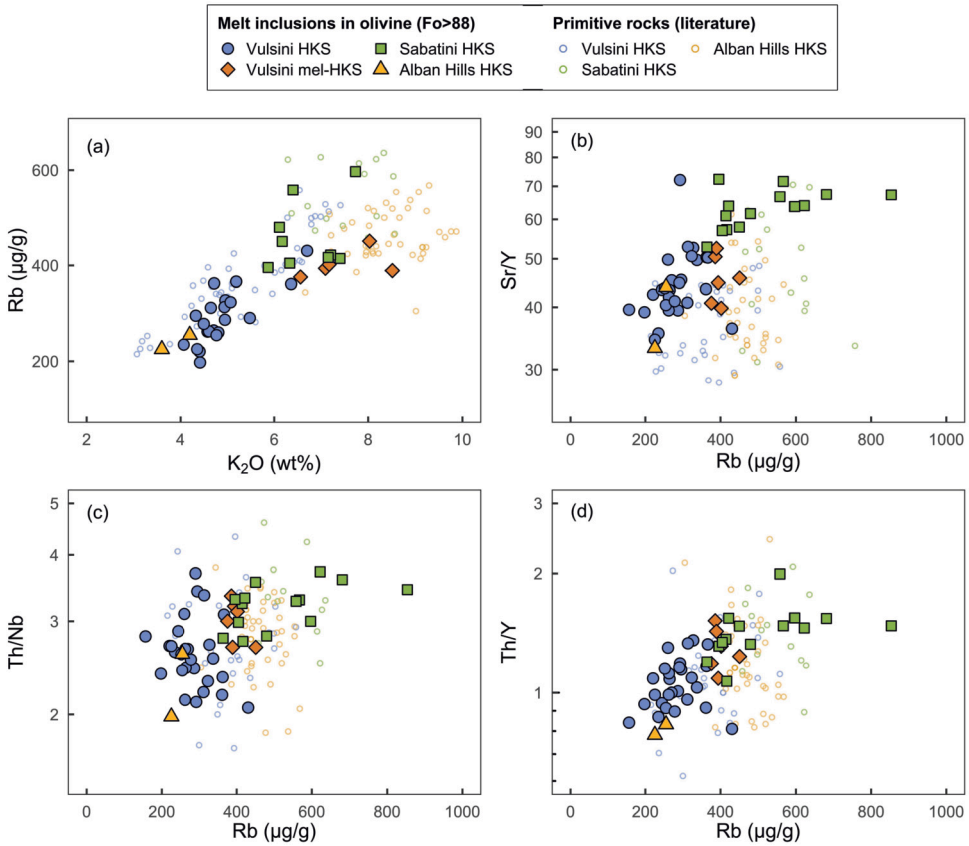

Fig. 7. Trace-element contents of Roman HKS melt inclusions. (a) K_2O (in wt%) versus Rb contents (in µg/g); and Rb contents versus (b) Sr/Y, (c) Th/Nb, and (d) Th/Y in melt inclusions hosted by olivines with Fo > 88 mol%. Ratios are plotted on logarithmic scales. Roman HKS primitive whole-rock data (MgO > 5 wt%, K_2O/Na_2O > 2, and LOI < 3 wt%; references as in Fig. 2) are shown for comparison.

6.2. A melt inclusion perspective on erupted lavas

Much has been written about the origin of the Roman ultrapotassic magmas on the basis of primitive whole-rock geochemistry, mineralogy, and petrography (e.g., Conticelli et al., 2010; Peccerillo, 2017, and references therein). This study presents the first major- and trace-element and Sr-Nd-Pb isotope data on Roman MIs; melts that have unequivocally been protected from shallow-level assimilation and magma fractionation beyond Fo_{88}. The MIs can therefore provide an important comparison to, and assessment of, whole-rock geochemical characteristics and, by extension, the source-related inferences that have been made on their basis.

For Vulsini HKS there is a first-order agreement between the data from the primitive bulk rocks and the MIs. Major- and trace-element and isotope compositions show very similar ranges (Figs. 4–8), with the difference being that the MIs, hosted by just six rock samples, cover virtually the entire spectrum of primitive Vulsini HKS lavas previously measured ($n = 74$). Overall, the MIs therefore seem to confirm the primitive characteristics of previously studied bulk lavas (Nappi et al., 1998; Di Battistini et al., 1998), though the melt and source heterogeneities have evidently been homogenised within the lavas.

A striking disparity is presented by Vulsini mel-HKS MIs, whose major-element compositions are extremely variable (Fig. 4) and exhibit ranges that are unlike the erupted melilite-bearing lavas (Di Battistini et al., 2001). Some of the MIs are much more incompatible-element enriched (e.g., in K, P, Ti) than the rocks. Their Sr-isotope composition (Fig. 8), whilst still within the range of primitive Vulsini lavas, is not an extension of the Vulsini HKS range, but instead significantly (~ 0.1%) higher.

Whilst primitive rocks and MIs from Sabatini HKS share many compositional characteristics (Fig. 4), the CaO concentrations of the MIs are higher and not inversely correlated with K_2O, and Al_2O_3 tends to be low. The MIs, hosted by just one rock sample, are also variable in K_2O (6–8 wt%). Some of the MIs show P_2O_5 and TiO_2 values that exceed the whole-rock range (Fig. 4). On the whole, Sabatini HKS MIs share most first-order characteristics with the primitive rocks (e.g., Conticelli et al., 1997), even though the rock samples represent aggregated melts with reduced compositional variability.

The MIs from Alban Hills HKS have a conspicuously less-enriched character compared to the bulk rocks (~ 4 versus 7–10 wt% K_2O; Fig. 4). These MI compositions are virtually identical to Vulsini HKS. However, the small number of data points limits meaningful interpretation at present. The question remains as to whether these melts are representative of the majority of the melts parental to Alban Hills HKS lavas. If they are, the source of Alban Hills HKS is akin to that of Vulsini HKS, and the enrichment in K_2O (up to 10 wt%) of the erupted lavas (Peccerillo et al., 1984; Boari et al., 2009a) may be of secondary origin.

6.3. Temperatures of olivine crystallisation

The calculated temperatures of olivine-melt equilibrium represent the temperature of melt entrapment and by implication that of olivine crystallisation. These temperatures are shown in Fig. 9, and are different for each MI suite. If we consider the presence of H_2O in our melts—with values reaching up to at least 2 wt% in Roman HKS MIs (Supplementary Table S4)—we find that our olivine-melt equilibrium (i.e., crystallisation) temperatures are lowered by about 90 °C (Fig. 9; see also Danyushevsky et al., 2002b).

The preservation of extreme compositional diversity and incomplete mixing of melts suggests that the melt batches were trapped in growing olivines without having traversed a significant temperature gradient since their generation (similar to e.g., Nikogosian and van Bergen,

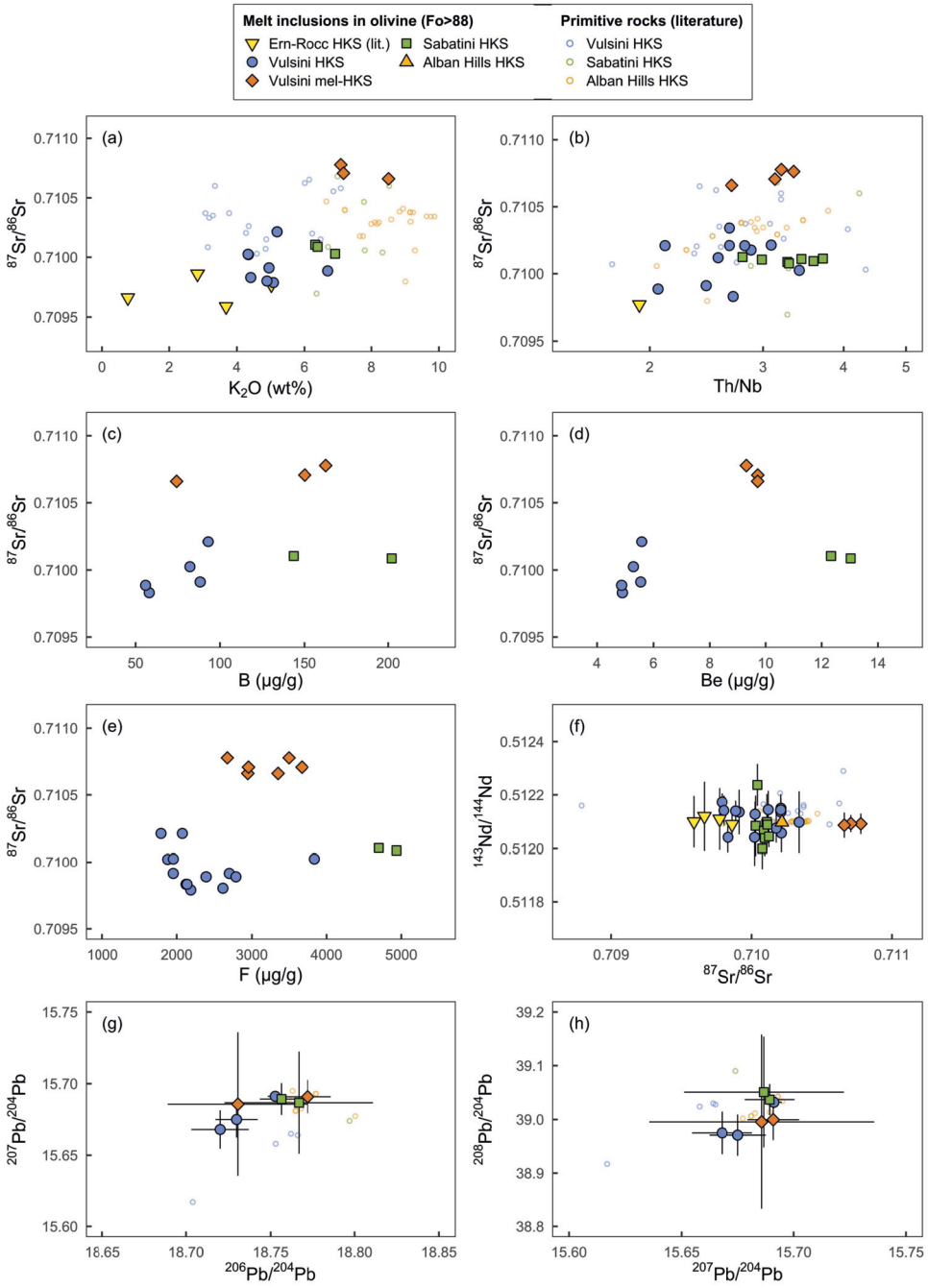

Fig. 8. Sr-Nd-Pb isotope compositions of Roman HKS melt inclusions. (a) K_2O contents (in wt%), (b) Th/Nb (in log scale), (c) B, (d) Be, and (e) F (in µg/g) versus $^{87}Sr/^{86}Sr$; (f) $^{87}Sr/^{86}Sr$ versus $^{143}Nd/^{144}Nd$; (g) $^{206}Pb/^{204}Pb$ versus $^{207}Pb/^{204}Pb$; and (h) $^{207}Pb/^{204}Pb$ versus $^{208}Pb/^{204}Pb$, all in melt inclusions hosted by olivines with Fo > 88 mol%. Ernici-Roccamonfina ("Ern-Rocc") HKS MI data (Fo > 88 mol%; K_2O/Na_2O > 2; Koornneef et al., 2019) and Roman HKS primitive whole-rock data (MgO > 5 wt%, K_2O/Na_2O > 2, and LOI < 3 wt%; references as in Fig. 2) are shown for comparison.

2010). Although the calculated crystallisation temperatures will not be identical to the melt generation temperatures, they are probably only a few tens of degrees lower. The highest equilibrium temperatures correspond to the lowest K_2O values (Vulsini HKS), and some of the lowest temperatures coincide with the highest K_2O contents (Vulsini mel-HKS). These observations support the idea that the most enriched melts, i.e., those with the highest proportion of melts derived from metasomatic domains, were generated at lower temperatures. This is consistent with experimental evidence showing that metasomatically-generated phase assemblages have significantly lower melting temperatures due to the presence of more fusible and/or hydrous phases (e.g., Foley, 1992; Foley et al., 1999, 2022a).

Foley et al. (2022a) show that the solidi for hydrous pyroxenites generating melts with 4–9 wt% K_2O at 15 kbar are about 1100–1150 °C—far below that of a dry lherzolite (Fig. 9). The Roman HKS melts fall roughly in the same realm as these solidi. However, it should be noted that our Roman HKS melts, which unlike the lamproite-generating experiments of Foley et al. (2022a), *do* require olivine in the source (Ammannati et al., 2016) and thus have a higher melting temperature than the solidi of olivine-free hydrous pyroxenites. Alternatively, the first melts to be generated could originate from olivine-free vein assemblages, and mix with peridotite-derived melts higher up in the melting region, yielding equilibrium temperatures that are integrated signatures of two different melting temperatures. The first-order sim-

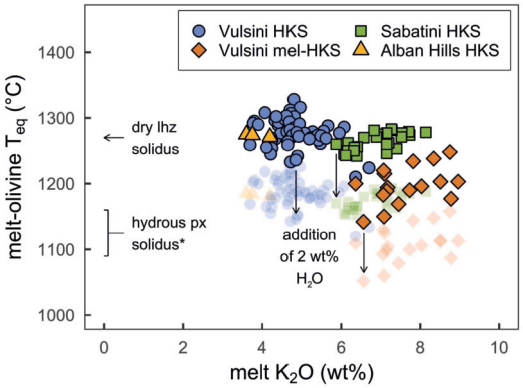

Fig. 9. Relation between melt K_2O contents and olivine crystallisation temperature. K_2O (in wt%) in olivine-hosted melt inclusions (Fo > 88 mol%) versus the olivine-melt equilibrium temperature (T_{eq} in °C; the inferred olivine crystallisation temperature). The translucent symbols illustrate the decrease in equilibrium temperature as a result of adding 2 wt% H_2O (calculated using Petrolog3; Danyushevsky and Plechov, 2011). The solidi of dry lherzolite ("dry lhz"; Katz et al., 2003) and experimental hydrous pyroxenites ("hydrous px") generating melts with 4–9 wt% K_2O at 15 kbar (Foley et al., 2022a) are shown for comparison.

ilarity of these temperatures, however, is compatible with the Roman HKS melts being extracted from a source containing hydrous phases. Moreover, the temperature variations also predict that, when exposed to heating, the first melts to be generated are the most enriched in K and associated elements. This is consistent with the vein-plus-wall-rock melting mechanism originally proposed by Foley (1992), in which melting starts in networks of 'veins' rich in clinopyroxene and mica, and progresses to the surrounding peridotite wall-rock, likely higher up in the melting region. Once the veins are exhausted and/or the temperature is increased above the melting point of the ambient mantle (i.e., peridotite), the enriched signature of the melts is progressively diluted. Theoretically, this could result in eruptive sequences with decreasing K-enrichment and related incompatible elements over time (e.g., from lamproite/kamafugite to HKS to KS to SHO to CA melts, or in part). Indeed, such temporal trends are observed in the Tuscan and Roman provinces, including Vulsini-Latera (Nikogosian and van Bergen, 2010; Conticelli et al., 2015; Peccerillo, 2017; Casalini et al., 2021).

6.4. Mixing between primitive melt components

We distinguish four MI suites in the Roman HKS province: Vulsini HKS, Vulsini mel-HKS, Sabatini HKS, and Alban Hills HKS. There are differences and variations both between and within these suites, which will be referred to as *inter*-suite and *intra*-suite, respectively.

As is evident from Figs. 4–8, the most notable inter-suite differences are those in K_2O, B, Be, and absolute trace-element contents, Sr/Y, Th/Nb, Th/Y ratios, and $^{87}Sr/^{86}Sr$, which clearly separate Vulsini HKS from Vulsini mel-HKS and Sabatini HKS. In turn, the difference between Vulsini mel-HKS and Sabatini HKS is clearest in Al_2O_3, P_2O_5, TiO_2, Be, F, Sr/Y, and $^{87}Sr/^{86}Sr$.

Intra-suite trends are evident for Vulsini HKS in terms of positive relationships between K_2O versus Al_2O_3, B, most trace elements, Sr/Y, and Th/Y. Covariations with $^{87}Sr/^{86}Sr$ are apparent for B and Be, but not directly with K_2O. For Vulsini mel-HKS, the large major-element variability is particularly apparent, especially in CaO and Al_2O_3. There are positive covariations between K_2O and Al_2O_3, P_2O_5, TiO_2, B, Be, and most trace elements. As evidenced by the difference in $^{87}Sr/^{86}Sr$, the chemical variations of Vulsini HKS and mel-HKS are *not* extensions of one another. Lastly, Sabatini HKS is a relatively invariable suite, with weak positive correlations between K_2O and CaO, TiO_2, and most trace elements, and negative covariations with SiO_2 and P_2O_5.

Although the data are somewhat scattered (Figs. 4–8), wherever present, these intra-suite trends appear to be linear and at first order are approximated by mixing between two components (or 'end-members') for each suite. As is evident from the variability in e.g., Fig. 4, at least three different enriched end-members are needed to explain Vulsini HKS, Vulsini mel-HKS, and Sabatini HKS, and at least one (common) depleted end-member is required. The enriched end-members principally differ in terms of K_2O, CaO, Al_2O_3, P_2O_5, TiO_2, B, Be, and absolute trace-element contents. Fig. 10 shows an example of three mixing lines that describe the intra-suite trends of Vulsini HKS, Vulsini mel-HKS, and Sabatini HKS.

The relatively constant $^{87}Sr/^{86}Sr$ values for Vulsini mel-HKS and Sabatini HKS (Fig. 8) indicate that the enriched components are likely to be very enriched in Sr compared to the depleted ('ambient') component. Binary mixing between the two is thus expected to give nearly constant $^{87}Sr/^{86}Sr$ values over a range of e.g., Sr and K_2O values because the enriched melt component will dominate the Sr budget and therefore the Sr isotope composition. The constant but different $^{87}Sr/^{86}Sr$ values of Vulsini mel-HKS and Sabatini HKS also imply that these melt suites are the products of individual, but different enriched components.

This raises the question of when the hybridisation of these components took place and what these end-members represent. Several studies have addressed this topic on the basis of bulk-rock compositions (Conticelli et al., 2007; Avanzinelli et al., 2009; Boari et al., 2009b; Conticelli et al., 2015). They surmised that the enriched melts are derived from metasomatic vein networks (end-member 1), subsequently diluted by less-enriched melts derived from the surrounding mantle (end-member 2)—the inference being that the end-members were mixed after melt generation. Neither of these end-members have erupted in their pure form. For instance, no pure peridotite-derived melts (and MIs) have been observed, from which can be concluded that the solidus temperature of ambient peridotite was not exceeded. Indeed, the original vein melting model of Foley (1992) had the vein-derived melts dissolving peridotite components at temperatures below its solidus.

The question remains whether the observed compositional spectrum of the MI suites represents the incomplete mixing of end-member melt batches or the heterogeneity of each end-member itself, be it in solid (i.e., mantle heterogeneity due to metasomatism) or liquid form (i.e., melt heterogeneity due to extraction processes). Nevertheless, the MIs reinforce the notion that the compositional spectrum of the Roman province melts is principally the result of a pre-magmatic phase of metasomatism, where the ambient mantle was modified by a liquid that reacted with the peridotite to form a locally heterogeneous metasomatic phase assemblage ('veins'). The composition and mineralogies of these veins are different for Vulsini HKS, Vulsini mel-HKS, and Sabatini HKS, resulting in three compositional suites. These suites represent the heterogeneity of the Roman province source domain as a result of differences in metasomatism. However, as per the model of Foley (1992), once extracted from the veins these liberated fluid-rich melts likely moved and locally induced melting of ambient peridotite at temperatures lower than their melting temperatures. This peridotite-derived component, which dilutes the pure vein signature, is likely to be broadly the same for each of the three compositional suites.

6.5. The mineral assemblage of the metasomatic veins

The most enriched melt components preserved in Vulsini HKS, Vulsini mel-HKS, and Sabatini HKS carry the most pristine evidence of the mineral assemblage of the metasomatic veins from which they were derived. However, even these enriched melts likely carry the integrated signature of the total melting assemblage, i.e., that emanating from the vein plus what is melted/dissolved from the surrounding peridotite (Foley, 1992; Conticelli et al., 2007; Avanzinelli et al., 2009; Boari et al., 2009b). Mantle xenoliths found in potassium-rich volcanic rocks are typically rich in mica + clinopyroxene ± amphibole (e.g., Grégoire et al., 2002; Fitzpayne et al., 2018), and rarely contain

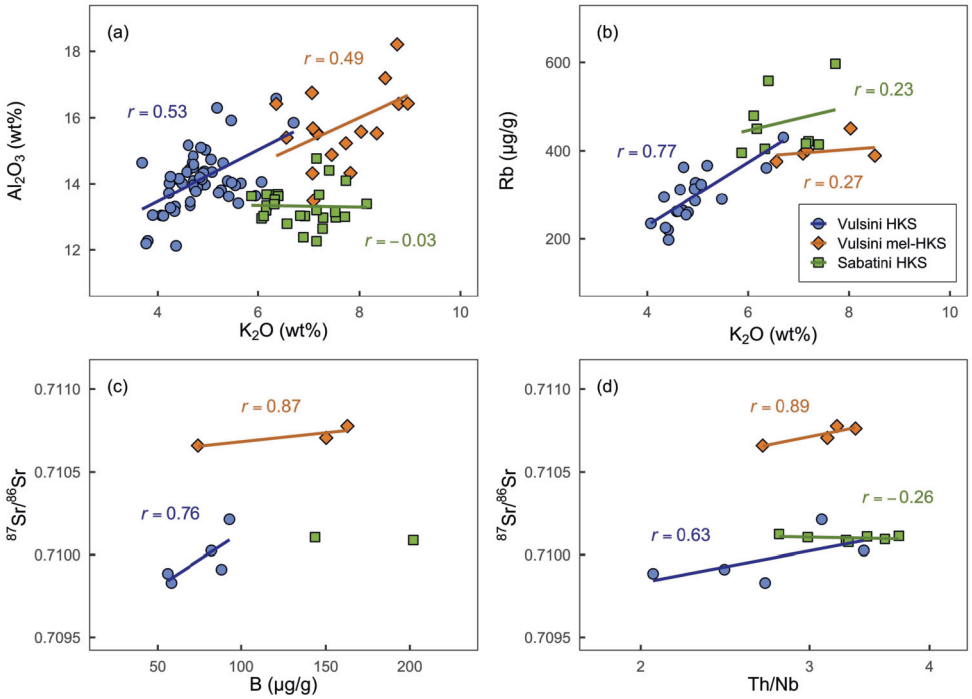

Fig. 10. Compositional variations within melt inclusion suites. K_2O (in wt%) versus (a) Al_2O_3 (in wt%) and (b) Rb (in µg/g), and (c) B (in µg/g) and (d) Th/Nb (in log scale) versus $^{87}Sr/^{86}Sr$ in olivine-hosted melt inclusions (Fo > 88 mol%; except Vulsini HKS: Fo > 90 mol%). Linear regression lines and Pearson correlation coefficient *r* are shown. See text for discussion.

olivine, consistent with experiments showing that both mica and (calcic and alkali) amphiboles melt incongruently under all known natural conditions and consume olivine when crystallising (Modreski and Boettcher, 1973; Gilbert et al., 1982; Condamine and Médard, 2014). The Roman HKS olivines have relatively low NiO (<0.4 wt%) and high CaO contents (0.2–0.8 wt%), which suggest that both olivine and clinopyroxene are part of the total melting assemblage, in agreement with Ammannati et al. (2016). However, the olivine signature likely derives principally from the surrounding peridotite and not the veins, because the compositions of the (ultra)potassic magmatism on the Italian peninsula indicate that the melting temperature of ambient peridotite was not exceeded. To start melting or dissolving the ambient peridotite, a hydrous melt—such as that derived from a metasomatic vein with a significantly lower solidus temperature—is needed (Foley, 1992). Clinopyroxene, however, was likely present in both the veins and the surrounding peridotite, but their relative abundances are challenging to constrain when the melts carry the integrated signature.

Fig. 11 summarises the inferred phase assemblages of the veins that gave rise to the enriched melt components of Vulsini HKS, Vulsini mel-HKS, and Sabatini HKS. The high K_2O contents (3–9 wt%) of the melts require a potassium-rich phase, such as phlogopite and/or the alkali amphibole K-richterite, to be a major constituent of the source. Experiments show that K-richterite melts rapidly and leads to a low-Al melt (Foley et al., 2022a), which is inconsistent with the high Al_2O_3 contents (12–18 wt%) of the Roman HKS melts. We therefore infer phlogopite, which also supplies Al, to be the principal host of K_2O for the Roman HKS, and constitute up to ~50% of the veins (Fig. 11).

The high Al_2O_3 contents coupled with high CaO (12–17 wt%) are indicative of calcic (Ca-)amphibole (e.g., Foley et al., 2022b). We infer Ca-amphibole, in addition to phlogopite, to account for much of the Al contents of the melts, and to make up 30 to 45% of the vein assemblage (Fig. 11). High CaO contents of the MIs, as well as their incompatible trace-element enrichment, are also compatible with a role for clinopyroxene, such as diopside, in the vein assemblage (~10–25%). The relative abundances of clinopyroxene (Ca ≫ Al), phlogopite (K, Al), and Ca-amphibole (Al, Ca ≫ K) were gauged by the different Ca/Al and K/Al of the enriched melt components (Fig. 11). In addition, both clinopyroxene and Ca-amphibole are suitable hosts for incompatible trace elements.

The principal differences between Vulsini mel-HKS and Vulsini HKS are best explained by higher proportions of phlogopite (~45% of the veins; increasing K, Al, F, and Rb) and Ca-amphibole (~45% of the veins; increasing Ca, Al, Ti, Na, and incompatible trace-element contents) in the mel-HKS veins (Fig. 11). This occurs at the expense of clinopyroxene (down to ~10%) in the vein as indicated by the mel-HKS melts, albeit variable, reaching lower CaO/Al_2O_3 values (down to 0.5). Additionally, the increase in P_2O_5 (up to 1.5 wt%), alongside high F (2700–3800 µg/g) and Cl contents (400–800 µg/g) in Vulsini mel-HKS, are compatible with apatite breakdown (~ 1%), which could simultaneously account for some of the enrichment in CaO and incompatible trace elements (Foley et al., 2022b). Variations in abundances of apatite and Ca-amphibole likely control the extreme variability of CaO and Al_2O_3 contents of Vulsini mel-HKS.

The lower Al_2O_3 contents of Sabatini HKS compared to Vulsini mel-HKS, at similar K_2O levels, indicate that there was less Ca-amphibole (~30% of the vein), but not less phlogopite, in the Sabatini veins. This is corroborated by their on average lower TiO_2 and Na_2O contents. The lower Al_2O_3 contents are not matched by lower CaO in Sabatini HKS (as would be expected for less Ca-amphibole), and their Sr/Y are higher than Vulsini mel-HKS. These observations are consistent with a greater proportion of clinopyroxene (up to ~25% of the vein). The higher Rb, F, and Be contents of Sabatini HKS suggest slightly more phlogopite in the veins (up to ~50% of the vein). Their similar K_2O contents may be accounted for by less K-bearing Ca-amphibole.

6.6. *The nature and provenance of the metasomatic agents*

Previous studies have inferred the nature (fluids vs. melts), provenance (carbonaceous vs. siliciclastic sediment recycling), and effects (vein generation and reaction) of the metasomatic agents underlying the complex mantle sources of Italian magmatism (e.g., Conticelli et al. 2007; Avanzinelli et al. 2009; Boari et al. 2009b; Conticelli et al.

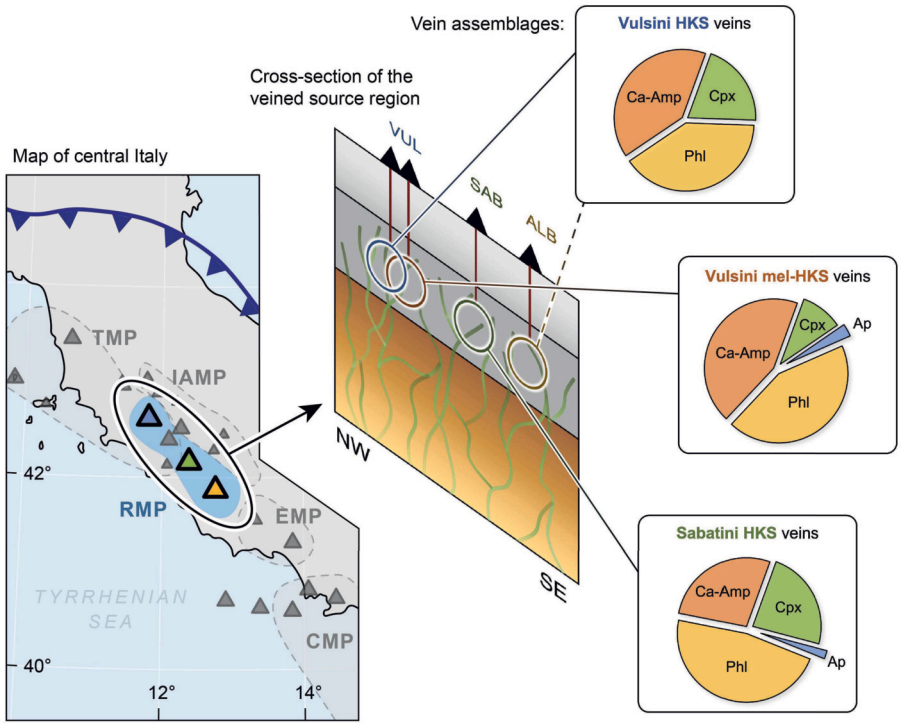

Fig. 11. Schematic display of the vein assemblages underlying the Roman province ultrapotassic magmatism. Map of central Italy (abbreviations as in Fig. 1) with a schematic NW-SE cross-section of the veined mantle source region with pie charts illustrating the inferred vein phase assemblages for Vulsini HKS, Vulsini melilite-bearing HKS, and Sabatini HKS. The vein assemblage for Alban Hills HKS is tentatively interpreted as being similar to Vulsini HKS (see text for discussion). Cpx = clinopyroxene; Phl = phlogopite; Ca-Amp = calcic amphibole; Ap = apatite.

2015; Ammannati et al. 2016). Trace-element and Sr-isotope compositions of the lavas indicate that the contaminants of the Roman province mantle source are carbonate-rich pelites, i.e., marls (Peccerillo et al., 1988; Peccerillo, 1998; Avanzinelli et al., 2009). Similarly, the low-Ni and high-Ca contents of Roman HKS olivines suggest a Ca-rich metasomatic agent derived from a recycled sedimentary carbonate (Ammannati et al., 2016). By contrast, the Tuscan lamproite source appears to require multiple metasomatism, involving the recycling of pelitic sediments and dehydration of lawsonite-bearing schists (Tommasini et al., 2011; Conticelli et al., 2015; Casalini et al., 2021). Variable Pb-isotope compositions of olivine-hosted melt inclusions from Latera also point to multiple metasomatic events beneath the region where the Tuscan and Roman provinces overlap (Nikogosian et al., 2016). In general, the metasomatic agents below Italy are thought to carry LILE, HFSE, and REE signatures that are strongly affected by the breakdown of accessory minerals (such as phengite, allanite, rutile, and ilmenite) at the slab-mantle wedge interface (e.g., Peccerillo and Frezzotti, 2015). Alternatively, the melting of imbricated metasediments at shallow depths (<80 km), with accessory minerals (such as lawsonite, phengite, titanite, and apatite) controlling the LILE, HFSE, and REE contents of the melts, has been suggested for potassium-rich volcanism in the Eastern Mediterranean (Wang et al., 2017, 2019).

The generation of the elevated Sr-isotope signature of the Roman province melts (>0.7098) requires the involvement of sediments that were either relatively old or Rb-rich when they melted to form the metasomatic agent, or requires Rb/Sr fractionation during sediment melting or metasomatic infiltration. The main piece of evidence to constrain the origin of the metasomatic liquids is the ~0.1% difference in $^{87}Sr/^{86}Sr$ between Vulsini HKS and Vulsini mel-HKS. If the subducted sediment had a Rb/Sr value of 1.1 (i.e., the maximum Rb/Sr reported for Eastern Mediterranean Sea sediments; Klaver et al., 2015) and melted completely ($F = 1$), the age difference required to generate this 0.1% offset is about 15 Myr. Highly fractionated Rb/Sr (>18) is needed to generate this offset from agents derived from sediments of similar (<1 Myr) age, but this degree of fractionation is unlikely to have been achieved during sediment melting, given $D_{Rb} = 0.7$ and $D_{Sr} = 0.25$ (Turner and Langmuir, 2022). Overall, the Sr-isotope difference implies that two different metasomatic agents have infiltrated the mantle region beneath Vulsini. These distinct metasomatic components could have originated from two different subduction systems (e.g., Alpine and Apennine) as argued for the mantle sources of Latera (Nikogosian et al., 2016) and Ernici-Roccamonfina (Koornneef et al., 2019). Alternatively, the disparate metasomatic agents could have originated from the same subducting slab but from different domains (depth and/or lateral position) in the slab, liberated at different P-T conditions and/or at different or multiple times. A lateral (trench-perpendicular) change in sediment composition could have been extracted progressively during ongoing westward subduction of the Adriatic plate since the Late Eocene beneath the present-day Roman province (Fig. 1). Alternatively, during slab breakoff or tearing, different parts of the (meta)sedimentary sequence could have become exposed to heat, and each sedimentary unit could have yielded a different metasomatic liquid with disparate elemental and Sr-isotope compositions. The movement of the subducted slab, such as that induced by rollback since the Late Eocene, could also have resulted in the slab experiencing different P-T conditions beneath the Roman province mantle source at different stages in time, yielding distinct metasomatic liquids.

The preservation of diversity in near-primary melt compositions beneath the Roman province also provides direct evidence that separates the metasomatism from the melting process in time. The erupted magmas clearly cannot be derived directly from the slab, as the upward movement of these melts would have homogenised any compositional diversity. The fact that the MIs must have been trapped close to their source region therefore necessitates the magmatism to have originated in two stages: (1) a metasomatic stage, during which agents were liberated from the subducted slab, infiltrated the mantle wedge, and reacted/precipitated to form a metasomatic phase assemblage, and (2) a melt generation stage, during which melting of this source was trig-

gered, possibly by a heat pulse associated with slab tearing (Spakman and Wortel, 2004; Rosenbaum et al., 2008). Thus, earlier inferences on the two-stage melting model for Italy (e.g., Peccerillo, 1999) are corroborated by the preservation of compositionally diverse batches of primitive melts.

6.7. Implications for the origin of ultrapotassic magmatism

Italy presents one of the most extreme and complex examples of potassium-rich post-collisional volcanism worldwide. Occurring in close spatial and temporal proximity, the wide variety of calc-alkaline to ultrapotassic, kamafugitic, and lamproitic magmas presents a unique but complex opportunity to better understand subduction recycling, metasomatism, and mantle heterogeneity worldwide.

One of the principal conclusions drawn from Italian MIs is that primary melts derived from metasomatised mantle sources are much more diverse than previously recognised. Italian MIs reveal melt compositions and source components unrepresented in bulk rocks (Nikogosian and van Bergen, 2010; Schiavi et al., 2012; Rose-Koga et al., 2012; Nikogosian et al., 2016; Koornneef et al., 2019, this study) and show that forsterite-rich olivine traps near-primary melts before they have accumulated and homogenised. MIs also characteristically show extended compositional ranges compared to bulk rocks, testifying that the erupted lavas are aggregated batches of diverse melts. As in this study, the lavas may effectively present compositional averages of the melt inclusions they contain. Hence, the identification of small-scale heterogeneities in the source of magmatism associated with subduction metasomatism benefits from the increased resolution that MIs offer.

Italian MIs, particularly when investigated for Sr-Nd-Pb isotopes, also demonstrate that multi-stage metasomatism is an important process underlying potassium-rich magmatism (Metrich et al., 1998; Schiavi et al., 2012; Nikogosian et al., 2016; Koornneef et al., 2019, this study). Superimposed subduction imprints may be derived from one or more subduction system(s) (Nikogosian et al., 2016; Koornneef et al., 2019, this study), and may be tapped millions of years later when exposed to a melting trigger. Melt mixing relations preserved in MI compositions reveal that multiple metasomatic components may be present even within a single (ultra)potassic volcanic district. As a result, the mantle domains in which these components are stored—the veins—can vary significantly in composition, mineralogy, mineral proportions and, ultimately, metasomatic provenance. Variations on such veined mantle sources are likely to underlie other complex potassium-rich occurrences in collision zones, such as the wider Alpine-Himalayan belt, South China, Central Asia, and Variscan orogens.

7. Summary

We present major-, volatile-, and trace-element and coupled Sr-Nd-Pb isotope data on olivine-hosted melt inclusions and major-element data on early-formed minerals (olivine, spinel) in primitive volcanic rocks from the Quaternary Roman magmatic province in central Italy to probe the mantle source and generation of ultrapotassic post-collisional magmatism.

- The early-formed minerals (olivine, spinel) and melt inclusions in olivine form compositional suites that correspond to the magmatic series of the host rocks: Vulsini HKS, Vulsini melilite-bearing HKS, Sabatini HKS, and Alban Hills HKS.
- Vulsini mel-HKS contains olivines with much higher CaO contents than Vulsini HKS, and Cr-spinel inclusions with higher Cr#. The compositions of the olivine-hosted MI suites form distinct populations: compared to Vulsini HKS, Vulsini mel-HKS and Sabatini HKS are enriched in K, P, Ti, volatiles (B, Be, F, Cl, S) and trace elements (absolute concentrations and Sr/Y, Th/Nb, and Th/Y), though there are also considerable differences between the latter two magmas. The principal difference is that in $^{87}Sr/^{86}Sr$ values between Sabatini HKS (as well as Vulsini HKS) and Vulsini mel-HKS, which is ~ 0.1%.
- The observed compositional variability in the MIs chiefly reflects the chemical heterogeneity of the primary melts during early olivine crystallisation, soon after melt extraction from the source region. The mantle source beneath the Roman magmatic province must therefore be chemically and lithologically heterogeneous, to a degree that was previously unknown.
- At least 3 different metasomatic vein types (i.e., veins with different compositions and mineralogies) are required to explain the compositional differences between Vulsini HKS, Vulsini mel-HKS, and Sabatini HKS, in addition to at least one depleted component, which is likely to be (hydrated) ambient peridotite.
- The mineral assemblage of the metasomatic veins consists of 40–50% phlogopite (supplying K, Al, F, and Rb), 30–45% Ca-amphibole (supplying Al, Ca, Ti, and Na), 10–25% clinopyroxene (supplying Ca), and 0–1% apatite (supplying P, Ca, F, and Cl). The enriched character of Vulsini mel-HKS compared to Vulsini HKS is due to a higher proportion of phlogopite and Ca-amphibole, and the presence of minor apatite. Sabatini HKS veins contain less Ca-amphibole than Vulsini mel-HKS, but more clinopyroxene and phlogopite.
- The Sr-isotopic differences between Vulsini mel-HKS and Vulsini HKS and Sabatini HKS cannot be the result of single-stage metasomatism or the melting process, and therefore require at least two distinct metasomatic events to have occurred beneath the Roman province. This could but need not be associated with two distinct subduction systems, as different metasomatic agents could have originated from different domains in the same subducting slab, liberated at different P-T-t conditions.

Declaration of competing interest

The authors declare that they have no known competing financial interests or personal relationships that could have appeared to influence the work reported in this paper.

Acknowledgements

We thank Manfred van Bergen, Roel van Elsas, Natascia Luciani, Helen de Waard, Tilly Bouten, Sergei Matveev, and Kirsten van Zuilen for their help. We thank Stephen Foley, Sandro Conticelli, and an anonymous reviewer for their constructive and insightful comments, and Rosemary Hickey-Vargas for efficient editorial handling. This research received funding from the European Research Council (ERC) under the European Union's Horizon 2020 research and innovation programme (grant agreement n° 759563).

Appendix A. Supplementary material

Supplementary material related to this article can be found online at https://doi.org/10.1016/j.gca.2023.06.012.

References

Allègre, C.J., Turcotte, D.L., 1986. Implications of a two-component marble-cake mantle. Nature 323, 123–127. https://doi.org/10.1038/323123a0.

Ammannati, E., Jacob, D., Avanzinelli, R., Foley, S.F., Conticelli, S., 2016. Low Ni olivine in silica-undersaturated ultrapotassic igneous rocks as evidence for carbonate metasomatism in the mantle. Earth Planet. Sci. Lett. 444, 64–74. https://doi.org/10.1016/j.epsl.2016.03.039.

Arai, S., 1994. Characterization of spinel peridotites by olivine-spinel compositional relationships: review and interpretation. Chem. Geol. 113, 191–204. https://doi.org/10.1016/0009-2541(94)90066-3.

Avanzinelli, R., Elliott, T., Tommasini, S., Conticelli, S., 2008. Constraints on the genesis of potassium-rich Italian volcanic rocks from U/Th disequilibrium. J. Petrol. 49, 195–223. https://doi.org/10.1093/petrology/egm076.

Avanzinelli, R., Lustrino, M., Mattei, M., Melluso, L., Conticelli, S., 2009. Potassic and ultrapotassic magmatism in the circum-Tyrrhenian region: significance of carbonated pelitic vs. pelitic sediment recycling at destructive plate margins. Lithos 113, 213–227. https://doi.org/10.1016/j.lithos.2009.03.029.

Beccaluva, L., Di Girolamo, P., Serri, G., 1991. Petrogenesis and tectonic setting of the Roman Volcanic Province, Italy. Lithos 26, 191–221. https://doi.org/10.1016/0024-4937(91)90029-K.

Boari, E., Avanzinelli, R., Melluso, L., Giordano, G., Mattei, M., De Benedetti, A.A., Morra, V., Conticelli, S., 2009a. Isotope geochemistry (Sr–Nd–Pb) and petrogenesis of leucite-bearing volcanic rocks from "Colli Albani" volcano, Roman Magmatic Province, Central Italy: inferences on volcano evolution and magma genesis. Bull. Volcanol. 71, 977–1005. https://doi.org/10.1007/s00445-009-0278-6.

Boari, E., Tommasini, S., Laurenzi, M., Conticelli, S., 2009b. Transition from ultrapotassic kamafugitic to sub-alkaline magmas: Sr, Nd, and Pb isotope, trace element and 40Ar-39Ar age data from the Middle Latin Valley volcanic field, Roman Magmatic Province, Central Italy. J. Petrol. 50, 1327–1357. https://doi.org/10.1093/petrology/egp003.

Brai, A., Piro, M., Trigila, R., 1979. Studio geopetrografico del complesso vulcanico di Latera (vulcani Vulsini): Nota III: I termini lavici dell'attività intracalderica finale. Period. Mineral. 48, 205–254.

Carminati, E., Lustrino, M., Doglioni, C., 2012. Geodynamic evolution of the central and western Mediterranean: tectonics vs. igneous petrology constraints. Tectonophysics 579, 173–192. https://doi.org/10.1016/j.tecto.2012.01.026.

Casalini, M., Avanzinelli, R., Tommasini, S., Natali, C., Bianchini, G., Prelević, D., Mattei, M., Conticelli, S., 2021. Petrogenesis of Mediterranean lamproites and associated rocks: the role of overprinted metasomatic events in the post-collisional lithospheric upper mantle. Geol. Soc. (Lond.) Spec. Publ. 513, 271–296. https://doi.org/10.1144/SP513-2021-36.

Chiarabba, C., Chiodini, G., 2013. Continental delamination and mantle dynamics drive topography, extension and fluid discharge in the Apennines. Geology 41, 715–718. https://doi.org/10.1130/G33992.1.

Civetta, L., Carmine, P., Manetti, P., Peccerillo, A., Poli, G., 1984. Petrology, geochemistry and Sr-isotope characteristics of lavas from the area of Commenda (Mts. Vulsini, Italy). Bull. Volcanol. 47, 581–595. https://doi.org/10.1007/BF01961228.

Class, C., Miller, D.M., Goldstein, S.L., Langmuir, C.H., 2000. Distinguishing melt and fluid subduction components in Umnak Volcanics, Aleutian Arc. Geochem. Geophys. Geosyst. 1. https://doi.org/10.1029/1999GC000010.

Condamine, P., Médard, E., 2014. Experimental melting of phlogopite-bearing mantle at 1 GPa: implications for potassic magmatism. Earth Planet. Sci. Lett. 397, 80–92. https://doi.org/10.1016/j.epsl.2014.04.027.

Conticelli, S., Avanzinelli, R., Ammannati, E., Casalini, M., 2015. The role of carbon from recycled sediments in the origin of ultrapotassic igneous rocks in the Central Mediterranean. Lithos 232, 293–299. https://doi.org/10.1016/j.lithos.2015.07.002.

Conticelli, S., Carlson, R.W., Widom, E., Serri, G., 2007. Chemical and isotopic composition (Os, Pb, Nd, and Sr) of Neogene to Quaternary calc-alkalic, shoshonitic, and ultrapotassic mafic rocks from the Italian peninsula: Inferences on the nature of their mantle sources. In: Beccaluva, L., Bianchini, G., Wilson, M. (Eds.), Cenozoic Volcanism in the Mediterranean Area: Geological Society of America Special Paper, vol. 418. Geological Society of America, pp. 171–202. https://doi.org/10.1130/2007.2418(09).

Conticelli, S., D'Antonio, M., Pinarelli, L., Civetta, L., 2002. Source contamination and mantle heterogeneity in the genesis of Italian potassic and ultrapotassic volcanic rocks: Sr-Nd-Pb isotope data from Roman Province and Southern Tuscany. Mineral. Petrol. 74, 189–222. https://doi.org/10.1007/s007100200004.

Conticelli, S., Francalanci, L., Manetti, P., Peccerillo, A., 1987. Evolution of Latera volcano, Vulsinian district (central Italy): stratigraphical and petrological data. Period. Mineral. 56, 175–199.

Conticelli, S., Francalanci, L., Manetti, P., Peccerillo, A., Santo, A., 1986. Caratteristiche composizionali dei prodotti dell'apparato di Latera (Monti Vulsini, Lazio Settentrionale) e loro significato vulcanologico. Mem. Soc. Geol. Ital. 35, 715–726.

Conticelli, S., Francalanci, L., Manetti, P., Raffaello, C., Sbrana, A., 1997. Petrology and geochemistry of the ultrapotassic rocks from the Sabatini Volcanic District, central Italy: the role of evolutionary processes in the genesis of variably enriched alkaline magmas. J. Volcanol. Geotherm. Res. 75, 107–136. https://doi.org/10.1016/S0377-0273(96)00062-5.

Conticelli, S., Francalanci, L., Santo, A., 1991. Petrology of final-stage Latera lavas (Vulsini Mts.): mineralogical, geochemical and Sr-isotopic data and their bearing on the genesis of some potassic magmas in central Italy. J. Volcanol. Geotherm. Res. 46, 187–212. https://doi.org/10.1016/0377-0273(91)90083-C.

Conticelli, S., Laurenzi, M., Giordano, G., Mattei, M., Avanzinelli, R., Melluso, L., Tommasini, S., Boari, E., Cifelli, F., Perini, G., 2010. Leucite-bearing (kamafugitic/leucititic) and -free (lamproitic) ultrapotassic rocks and associated shoshonites from Italy: constraints on petrogenesis and geodynamics. J. Virtual Explorer 36. https://doi.org/10.3809/jvirtex.2009.00251.

Conticelli, S., Melluso, L., Perini, G., Avanzinelli, R., Boari, E., 2004. Petrologic, geochemical and isotopic characteristics of potassic and ultrapotassic magmatism in central-southern Italy: inferences on its genesis and on the nature of mantle sources. Period. Mineral. 73, 153–164.

Conticelli, S., Peccerillo, A., 1992. Petrology and geochemistry of potassic and ultrapotassic volcanism in central Italy: petrogenesis and inferences on the evolution of the mantle sources. Lithos 28, 221–240. https://doi.org/10.1016/0024-4937(92)90008-M.

Danyushevsky, L., Della-Pasqua, F., Sokolov, S., 2000. Re-equilibration of melt inclusions trapped by magnesian olivine phenocrysts from subduction-related magmas: petrological implications. Contrib. Mineral. Petrol. 138, 68–83. https://doi.org/10.1007/PL00007664.

Danyushevsky, L., Plechov, P., 2011. Petrolog3: integrated software for modeling crystallization processes. Geochem. Geophys. Geosyst. 12. https://doi.org/10.1029/2011GC003516.

Danyushevsky, L.V., McNeill, A.W., Sobolev, A.V., 2002a. Experimental and petrological studies of melt inclusions in phenocrysts from mantle-derived magmas: an overview of techniques, advantages and complications. Chem. Geol. 183, 5–24. https://doi.org/10.1016/S0009-2541(01)00369-2.

Danyushevsky, L.V., Sobolev, A.V., 1996. Ferric-ferrous ratio and oxygen fugacity calculations for primitive mantle-derived melts: calibration of an empirical technique. Mineral. Petrol. 57, 229–241. https://doi.org/10.1007/BF01162360.

Danyushevsky, L.V., Sokolov, S., Falloon, T.J., 2002b. Melt inclusions in olivine phenocrysts: Using diffusive re-equilibration to determine the cooling history of a crystal, with implications for the origin of olivine-phyric volcanic rocks. J. Petrol. 43, 1651–1671. https://doi.org/10.1093/petrology/43.9.1651.

Di Battistini, G., Montanini, A., Vernia, L., Bargossi, G.M., Castorina, F., 1998. Petrology and geochemistry of ultrapotassic rocks from the Montefiascone Volcanic Complex (Central Italy): magmatic evolution and petrogenesis. Lithos 43, 169–195. https://doi.org/10.1016/S0024-4937(98)00013-9.

Di Battistini, G., Montanini, A., Vernia, L., Venturelli, G., Tonarini, S., 2001. Petrology of melilite-bearing rocks from the Montefiascone Volcanic Complex (Roman Magmatic Province): new insights into the ultrapotassic volcanism of Central Italy. Lithos 59, 1–24. https://doi.org/10.1016/S0024-4937(01)00054-8.

Di Rocco, T., Freda, C., Gaeta, M., Mollo, S., Dallai, L., 2012. Magma chambers emplaced in carbonate substrate: petrogenesis of skarn and cumulate rocks and implications for CO2 degassing in volcanic areas. J. Petrol. 53, 2307–2332. https://doi.org/10.1093/petrology/egs051.

Faccenna, C., Becker, T., Pio Lucente, F., Jolivet, L., Rossetti, F., 2001. History of subduction and back-arc extension in the Central Mediterranean. Geophys. J. Int. 145, 809–820. https://doi.org/10.1046/j.0956-540x.2001.01435.x.

Fitzpayne, A., Giuliani, A., Hergt, J., Phillips, D., Janney, P., 2018. New geochemical constraints on the origins of MARID and PIC rocks: implications for mantle metasomatism and mantle-derived potassic magmatism. Lithos 318–319, 478–493. https://doi.org/10.1016/j.lithos.2018.08.036.

Foley, S., 1992. Vein-plus-wall-rock melting mechanisms in the lithosphere and the origin of potassic alkaline magmas. Lithos 28, 435–453. https://doi.org/10.1016/0024-4937(92)90018-T.

Foley, S.F., Ezad, I.S., van der Laan, S.R., Pertermann, M., 2022a. Melting of hydrous pyroxenites with alkali amphiboles in the continental mantle: 1. Melting relations and major element compositions of melts. Geosci. Front. 13, 101380. https://doi.org/10.1016/j.gsf.2022.101380.

Foley, S.F., Ezad, I.S., van der Laan, S.R., Shu, C., 2022b. Major and trace element compositions of partial melts of hydrous pyroxenites and their relationship to volcanism and mantle evolution. In: Goldschmidt Abstracts. European Association of Geochemistry, France. https://doi.org/10.46427/gold2022.11550.

Foley, S.F., Musselwhite, D.S., van der Laan, S.R., 1999. Melt compositions from ultramafic vein assemblages in the lithospheric mantle: a comparison of cratonic and non-cratonic settings. In: Proceedings of the 7th International Kimberlite Conference. Red Roof Design, Cape Town, South Africa, pp. 238–246.

Foley, S.F., Venturelli, G., Green, D.H., Toscani, L., 1987. The ultrapotassic rocks: characteristics, classification, and constraints for petrogenetic models. Earth-Sci. Rev. 24, 81–134. https://doi.org/10.1016/0012-8252(87)90001-8.

Ford, C., Russell, D., Craven, J., Fisk, M., 1983. Olivine-liquid equilibria: temperature, pressure and composition dependence of the crystal/liquid cation partition coefficients for Mg, Fe2+, Ca and Mn. J. Petrol. 24, 256–266. https://doi.org/10.1093/petrology/24.3.256.

Freda, C., Gaeta, M., Palladino, D., Trigila, R., 1997. The Villa Senni Eruption (Alban Hills, central Italy): the role of H2O and CO2 on the magma chamber evolution and on the eruptive scenario. J. Volcanol. Geotherm. Res. 78, 103–120. https://doi.org/10.1016/S0377-0273(97)00007-3.

Gaeta, M., Di Rocco, T., Freda, C., 2009. Carbonate assimilation in open magmatic systems: the role of melt-bearing skarns and cumulate-forming processes. J. Petrol. 50, 361–385. https://doi.org/10.1093/petrology/egp002.

Gasperini, D., Blichert-Toft, J., Bosch, D., Del Moro, A., Macera, P., Albarède, F., 2002. Upwelling of deep mantle material through a plate window: evidence from the geochemistry of Italian basaltic volcanics. J. Geophys. Res., Solid Earth 107, 2367. https://doi.org/10.1029/2001JB000418.

Giacomuzzi, G., Civalleri, M., De Gori, P., Chiarabba, C., 2012. A 3D vs model of the upper mantle beneath Italy: insight on the geodynamics of central Mediterranean. Earth Planet. Sci. Lett. 335–336, 105–120. https://doi.org/10.1016/j.epsl.2012.05.004.

Gilbert, M.C., Helz, R.T., Popp, R.K., Spear, F.S., 1982. Experimental studies of amphibole stability. In: Veblen, D.R., Ribbe, P.H. (Eds.), Amphiboles: Petrology and Experimental Phase Relations. Reviews in Mineralogy, 9B. Mineralogical Society of America, pp. 229–353, chapter 2. https://doi.org/10.2138/rmg.1982.10.2.

Giordano, G., De Benedetti, A., Diana, A., Diano, G., Gaudioso, F., Marasco, F., Miceli, M., Mollo, S., Cas, R., Funiciello, R., 2006. The Colli Albani mafic caldera (Roma, Italy): stratigraphy, structure and petrology. J. Volcanol. Geotherm. Res. 155, 49–80. https://doi.org/10.1016/j.jvolgeores.2006.02.009.

Grégoire, M., Bell, D., Le Roex, A., 2002. Trace element geochemistry of phlogopite-rich mafic mantle xenoliths: their classification and their relationship to phlogopite-bearing peridotites and kimberlites revisited. Contrib. Mineral. Petrol. 142, 603–625. https://doi.org/10.1007/s00410-001-0315-8.

Hanson, G.N., 1977. Geochemical evolution of the suboceanic mantle. J. Geol. Soc. 134, 235–253. https://doi.org/10.1144/gsjgs.134.2.0235.

Harte, B., 1987. Metasomatic events recorded in mantle xenoliths: an overview. In: Mantle Xenoliths, pp. 625–640.

van Hinsbergen, D.J.J., Torsvik, T.H., Schmid, S.M., Maţenco, L.C., Maffione, M., Vissers, R.L.M., Gürer, D., Spakman, W., 2020. Orogenic architecture of the Mediterranean region and kinematic reconstruction of its tectonic evolution since the Triassic. Gondwana Res. 81, 79–229. https://doi.org/10.1016/j.gr.2019.07.009.

van Hinsbergen, D.J.J., Vissers, R.L.M., Spakman, W., 2014. Origin and consequences of western Mediterranean subduction, rollback, and slab segmentation. Tectonics 33, 393–419. https://doi.org/10.1002/2013TC003349.

de Hoog, J.C.M., Mason, P.R.D., van Bergen, M.J., 2001. Sulfur and chalcophile elements in subduction zones: constraints from a laser ablation ICP-MS study of melt inclusions from Galunggung volcano, Indonesia. Geochim. Cosmochim. Acta 65, 3147–3164. https://doi.org/10.1016/S0016-7037(01)00634-2.

Jochum, K.P., Stoll, B., Herwig, K., Willbold, M., Hofmann, A.W., Amini, M., Aarburg, S., Abouchami, W., Hellebrand, E., Mocek, B., 2006. MPI-DING reference glasses for in situ microanalysis: new reference values for element concentrations and isotope ratios. Geochem. Geophys. Geosyst. 7. https://doi.org/10.1029/2005GC001060.

Jochum, K.P., Weis, U., Stoll, B., Kuzmin, D., Yang, Q., Raczek, I., Jacob, D.E., Stracke, A., Birbaum, K., Frick, D.A., Günther, D., Enzweiler, J., 2011. Determination of reference values for NIST SRM 610-617 glasses following ISO guidelines. Geostand. Geoanal. Res. 35, 397–429. https://doi.org/10.1111/j.1751-908X.2011.00120.x.

Kamenetsky, V., Métrich, N., Cioni, R., 1995. Potassic primary melts of Vulsini (Roman Province): evidence from mineralogy and melt inclusions. Contrib. Mineral. Petrol. 120, 186–196. https://doi.org/10.1007/BF00287116.

Karner, D.B., Marra, F., Renne, P.R., 2001. The history of the Monti Sabatini and Alban Hills volcanoes: groundwork for assessing volcanic-tectonic hazards for Rome. J. Volcanol. Geotherm. Res. 107, 185–219. https://doi.org/10.1016/S0377-0273(00)00258-4.

Katz, R.F., Spiegelman, M., Langmuir, C.H., 2003. A new parameterization of hydrous mantle melting. Geochem. Geophys. Geosyst. 4, 1073. https://doi.org/10.1029/2002GC000433.

Klaver, M., Djuly, T., de Graaf, S., Sakes, A., Wijbrans, J., Davies, G., Vroon, P., 2015. Temporal and spatial variations in provenance of Eastern Mediterranean Sea sediments: implications for Aegean and Aeolian arc volcanism. Geochim. Cosmochim. Acta 153, 149–168. https://doi.org/10.1016/j.gca.2015.01.007.

Klaver, M., Smeets, R.J., Koornneef, J.M., Davies, G.R., Vroon, P.Z., 2016. Pb isotope analysis of ng size samples by TIMS equipped with a 1013 Ω resistor using a 207Pb–204Pb double spike. J. Anal. At. Spectrom. 31, 171–178. https://doi.org/10.1039/C5JA00130G.

Koornneef, J.M., Bouman, C., Schwieters, J.B., Davies, G.R., 2014. Measurement of small ion beams by thermal ionisation mass spectrometry using new 1013 ohm resistors. Anal. Chim. Acta 819, 49–55. https://doi.org/10.1016/j.aca.2014.02.007.

Koornneef, J.M., Nikogosian, I., van Bergen, M.J., Vroon, P.Z., Davies, G.R., 2019. Ancient recycled lower crust in the mantle source of recent Italian magmatism. Nat. Commun. 10, 1–10. https://doi.org/10.1038/s41467-019-11072-5.

Koornneef, J.M., Nikogosian, I.K., van Bergen, M.J., Smeets, R., Bouman, C., Davies, G.R., 2015. TIMS analysis of Sr and Nd isotopes in melt inclusions from Italian potassium-rich lavas using prototype 1013 Ω amplifiers. Chem. Geol. 397, 14–23. https://doi.org/10.1016/j.chemgeo.2015.01.005.

Manning, C., 2004. The chemistry of subduction-zone fluids. Earth Planet. Sci. Lett. 223, 1–16. https://doi.org/10.1016/j.epsl.2004.04.030.

Marra, F., Karner, D.B., Freda, C., Gaeta, M., Renne, P., 2009. Large mafic eruptions at Alban Hills volcanic cistrict (central Italy): chronostratigraphy, petrography and eruptive behavior. J. Volcanol. Geotherm. Res. 179, 217–232. https://doi.org/10.1016/j.jvolgeores.2008.11.009.

Mason, P.R.D., Nikogosian, I.K., van Bergen, M.J., 2008. Major and trace element analysis of melt inclusions by laser ablation ICP-MS. In: Laser Ablation ICP-MS in the Earth Sciences: Current Practices and Outstanding Issues: Mineralogical Association of Canada Short Course Series, vol. 40, pp. 219–240.

Masotta, M., Mollo, S., Gaeta, M., Freda, C., 2016. Melt extraction in mush zones: The case of crystal-rich enclaves at the Sabatini Volcanic District (central Italy). Lithos 248–251, 288–292. https://doi.org/10.1016/j.lithos.2016.01.030.

Maurel, C., Maurel, P., 1982. Étude expérimentale de l'équilibre Fe2+-Fe3+ dans les spinelles chromifères et les liquides silicatés basiques coexistants, à 1 atm. C. R. Acad. Sci. 295, 209–212.

McDonough, W.F., Sun, S.-s., 1995. The composition of the Earth. Chem. Geol. 120, 223–253. https://doi.org/10.1016/0009-2541(94)00140-4.

Metrich, N., Joron, J.-L., Berthier, B., 1998. Occurrence of boron-rich potassic melts in the Vulsini volcanic district, Italy: evidence from melt inclusions. Geochim. Cosmochim. Acta 62, 507–514. https://doi.org/10.1016/S0016-7037(97)00365-7.

Modreski, P.J., Boettcher, A.L., 1973. Phase relationships of phlogopite in the system K2O-MgO-CaO-Al2O3-SiO2-H2O to 35 kilobars: a better model for micas in the interior of the Earth. Am. J. Sci. 273, 385–414. https://doi.org/10.2475/ajs.273.5.385.

Nappi, G., Antonelli, F., Coltorti, M., Milani, L., Renzulli, A., Siena, F., 1998. Volcanological and petrological evolution of the eastern Vulsini district, central Italy. J. Volcanol. Geotherm. Res. 87, 211–232. https://doi.org/10.1016/S0377-0273(98)00093-6.

Nikogosian, I.K., van Bergen, M.J., 2010. Heterogeneous mantle sources of potassium-rich magmas in central-southern Italy: melt inclusion evidence from Roccamonfina and Ernici (Mid Latina Valley). J. Volcanol. Geotherm. Res. 197, 279–302. https://doi.org/10.1016/j.jvolgeores.2010.06.014.

Nikogosian, I.K., Elliott, T., Touret, J.L.R., 2002. Melt evolution beneath thick lithosphere: a magmatic inclusion study of La Palma, Canary Islands. Chem. Geol. 183, 169–193. https://doi.org/10.1016/S0009-2541(01)00387-4.

Nikogosian, I.K., Ersoy, Ö., Whitehouse, M.J., Mason, P.R.D., de Hoog, J.C.M., Wortel, M.J.R., van Bergen, M.J., 2016. Multiple subduction imprints in the mantle below Italy detected in a single lava flow. Earth Planet. Sci. Lett. 449, 12–19. https://doi.org/10.1016/j.epsl.2016.05.033.

Peccerillo, A., 1998. Relationships between ultrapotassic and carbonate-rich volcanic rocks in central Italy: petrogenetic and geodynamic implications. Lithos 43, 267–279. https://doi.org/10.1016/S0024-4937(98)00016-4.

Peccerillo, A., 1999. Multiple mantle metasomatism in central-southern Italy: geochemical effects, timing and geodynamic implications. Geology 27, 315–318. https://doi.org/10.1130/0091-7613(1999)027<0315:MMMICS>2.3.CO;2.

Peccerillo, A., 2003. Plio-Quaternary magmatism in Italy. Episodes 26, 222–226. https://doi.org/10.18814/epiiugs/2003/v26i3/012.

Peccerillo, A., 2017. Cenozoic Volcanism in the Tyrrhenian Sea Region, 2nd ed. Advances in Volcanology. Springer International Publishing, Cham. https://doi.org/10.1007/978-3-319-42491-0.

Peccerillo, A., Federico, M., Barbieri, M., Brilli, M., Wu, T.-W., 2010. Interaction between ultrapotassic magmas and carbonate rocks: evidence from geochemical and isotopic (Sr, Nd, O) compositions of granular lithic clasts from the Alban Hills Volcano, Central Italy. Geochim. Cosmochim. Acta 74, 2999–3022. https://doi.org/10.1016/j.gca.2010.02.021.

Peccerillo, A., Frezzotti, M., 2015. Magmatism, mantle evolution and geodynamics at the converging plate margins of Italy. J. Geol. Soc. 172, 407–427. https://doi.org/10.1144/jgs2014-085.

Peccerillo, A., Poli, G., Serri, G., 1988. Petrogenesis of orenditic and kamafugitic rocks from central Italy. Can. Mineral. 26, 45–65.

Peccerillo, A., Poli, G., Tolomeo, L., 1984. Genesis, evolution and tectonic significance of K-rich volcanics from the Alban Hills (Roman comagmatic region) as inferred from trace element geochemistry. Contrib. Mineral. Petrol. 86, 230–240. https://doi.org/10.1007/BF00373668.

Plank, T., 2014. The chemical composition of subducting sediments. In: Holland, H., Turekian, K. (Eds.), Treatise on Geochemistry, 2nd ed. Elsevier, pp. 607–629, chapter 4.17. https://doi.org/10.1016/B978-0-08-095975-7.00319-3.

Plank, T., Langmuir, C., 1998. The chemical composition of subducting sediment and its consequences for the crust and mantle. Chem. Geol. 145, 325–394. https://doi.org/10.1016/S0009-2541(97)00150-2.

Portnyagin, M., Hoernle, K., Plechov, P., Mironov, N., Khubunaya, S., 2007. Constraints on mantle melting and composition and nature of slab components in volcanic arcs from volatiles (H2O, S, Cl, F) and trace elements in melt inclusions from the Kamchatka Arc. Earth Planet. Sci. Lett. 255, 53–69. https://doi.org/10.1016/j.epsl.2006.12.005.

Rogers, N.W., Hawkesworth, C.J., Parker, R.J., Marsh, J.S., 1985. The geochemistry of potassic lavas from Vulsini, central Italy and implications for mantle enrichment processes beneath the Roman region. Contrib. Mineral. Petrol. 90, 244–257. https://doi.org/10.1007/BF00378265.

Rose-Koga, E., Koga, K., Schiano, P., Le Voyer, M., Shimizu, N., Whitehouse, M., Clocchiatti, R., 2012. Mantle source heterogeneity for South Tyrrhenian magmas revealed by Pb isotopes and halogen contents of olivine-hosted melt inclusions. Chem. Geol. 334, 266–279. https://doi.org/10.1016/J.CHEMGEO.2012.10.033.

Rosenbaum, G., Gasparon, M., Lucente, F., Peccerillo, A., Miller, M., 2008. Kinematics of slab tear faults during subduction segmentation and implications for Italian magmatism. Tectonics 27. https://doi.org/10.1029/2007TC002143.

Rudge, J.F., Maclennan, J., Stracke, A., 2013. The geochemical consequences of mixing melts from a heterogeneous mantle. Geochim. Cosmochim. Acta 114, 112–143. https://doi.org/10.1016/j.gca.2013.03.042.

Schiavi, F., Kobayashi, K., Nakamura, E., Tiepolo, M., Vannucci, R., 2012. Trace element and Pb–B–Li isotope systematics of olivine-hosted melt inclusions: insights into source metasomatism beneath Stromboli (southern Italy). Contrib. Mineral. Petrol. 163, 1011–1031. https://doi.org/10.1007/s00410-011-0713-5.

Serri, G., Innocenti, F., Manetti, P., 1993. Geochemical and petrological evidence of the subduction of delaminated Adriatic continental lithosphere in the genesis of the Neogene-Quaternary magmatism of central Italy. Tectonophysics 223, 117–147. https://doi.org/10.1016/0040-1951(93)90161-C.

Smith, D., Leeman, W., 2005. Chromian spinel–olivine phase chemistry and the origin of primitive basalts of the southern Washington Cascades. J. Volcanol. Geotherm. Res. 140, 49–66. https://doi.org/10.1016/j.jvolgeores.2004.07.015.

Sobolev, A.V., 1996. Melt inclusions in minerals as a source of principle petrological information. Petrology 4, 209–220.

Sottili, G., Arienzo, I., Castorina, F., Gaeta, M., Giaccio, B., Marra, F., Palladino, D.M., 2019. Time-dependent Sr and Nd isotope variations during the evolution of the ultrapotassic Sabatini Volcanic District (Roman province, Central Italy). Bull. Volcanol. 81, 67. https://doi.org/10.1007/s00445-019-1324-7.

Sottili, G., Palladino, D.M., Gaeta, M., Masotta, M., 2012. Origins and energetics of maar volcanoes: Examples from the ultrapotassic Sabatini Volcanic District (Roman Province, Central Italy). Bull. Volcanol. 74, 163–186. https://doi.org/10.1007/s00445-011-0506-8.

Sottili, G., Palladino, D.M., Marra, F., Jicha, B., Karner, D.B., Renne, P., 2010. Geochronology of the most recent activity in the Sabatini volcanic district, Roman Province, central Italy. J. Volcanol. Geotherm. Res. 196, 20–30. https://doi.org/10.1016/j.jvolgeores.2010.07.003.

Spakman, W., Wortel, M., 2004. Tomographic view on Western Mediterranean geodynamics. In: Cavazza, W., Roure, F., Spakman, W., Stampfli, G., Ziegler, P. (Eds.), The TRANSMED Atlas. The Mediterranean Region from Crust to Mantle. Springer, Berlin, Heidelberg, pp. 31–52, chapter 2. https://doi.org/10.1007/978-3-642-18919-7_2.

Spandler, C., Pirard, C., 2013. Element recycling from subducting slabs to arc crust: a review. Lithos 170–171, 208–223. https://doi.org/10.1016/j.lithos.2013.02.016.

Stracke, A., Bourdon, B., 2009. The importance of melt extraction for tracing mantle heterogeneity. Geochim. Cosmochim. Acta 73, 218–238. https://doi.org/10.1016/j.gca.2008.10.015.

Tommasini, S., Avanzinelli, R., Conticelli, S., 2011. The Th/La and Sm/La conundrum of the Tethyan realm lamproites. Earth Planet. Sci. Lett. 301, 469–478. https://doi.org/10.1016/j.epsl.2010.11.023.

Turner, S.J., Langmuir, C.H., 2022. Sediment and ocean crust both melt at subduction zones. Earth Planet. Sci. Lett. 584, 117424. https://doi.org/10.1016/j.epsl.2022.117424.

Varekamp, J.C., Kalamarides, R.I., 1989. Hybridization processes in leucite tephrites from Vulsini, Italy, and the evolution of the Italian potassic suite. J. Geophys. Res., Solid Earth 94, 4603–4618. https://doi.org/10.1029/JB094iB04p04603.

Vernia, L., Bargossi, G.M., Di Battistini, G., Montanini, A., 1995. Caratteri geopetrografici e vulcanologici del settore sud-orientale Vulsino (Montefiascone-Commenda, Viterbo). Boll. Soc. Geol. Ital. 114, 665–677.

Wang, Y., Prelević, D., Buhre, S., Foley, S.F., 2017. Constraints on the sources of post-collisional K-rich magmatism: The roles of continental clastic sediments and terrigenous blueschists. Chem. Geol. 455, 192–207. https://doi.org/10.1016/j.chemgeo.2016.10.006.

Wang, Y., Prelević, D., Foley, S.F., 2019. Geochemical characteristics of lawsonite blueschists in tectonic mélange from the Tavşanlı Zone, Turkey: potential constraints on the origin of Mediterranean potassium-rich magmatism. Am. Mineral. 104, 724–743. https://doi.org/10.2138/am-2019-6818.

Wortel, M.J.R., Spakman, W., 2000. Subduction and slab detachment in the Mediterranean-Carpathian region. Science 290, 1910–1917. https://doi.org/10.1126/science.290.5498.1910.